

# A Tutorial on the Tracking, Telemetry, and Command (TT&C) for Space Missions

Andrea Modenini<sup>1</sup>, Barbara Ripani<sup>2</sup>, *Student Member, IEEE*

**Abstract**—This paper presents a tutorial on the Tracking, Telemetry, and Command (TT&C) for spacecraft and satellite missions. In particular, it provides a thorough summary of the design of the TT&C, starting from elementary system aspects and going down to the details of the on-board TT&C subsystem design, its units, and the physical layer. The paper is then complemented with a description of emerging TT&C techniques and technologies, the standardization framework, and with practical examples of actual spacecraft design of European space missions.

The tutorial here presented is thought for professionals (also in other telecommunication engineering fields) that want to face the challenges and state-of-the-art of the TT&C, and know more about this fundamental function that allows us to daily control and monitor our spacecraft.

**Index terms**—TT&C, PDT, Telecommand, Telemetry, Ranging, Transponder, Satellite

## I. INTRODUCTION

The TT&C is a critical function of the spacecraft that ensures the flying system operates correctly. As depicted in the sketch of Figure 1, the TT&C is done by means of radio-frequency (RF) links between the space element and the ground. As the name suggests, it performs three fundamental tasks: *Command* (also known as *telecommand*, TC), *Telemetry* (TM), and *Tracking* (also denoted, with abuse of naming, simply as *ranging*, RNG). The TC, trivially, is the function that allows to send commands and thus control the spacecraft: the mission operation center (MOC) sends commands through an Earth-to-space data burst transmission. Since commands are simple data that trigger specific spacecraft actions, TC data rates are usually in the order of some kbps (or even bps). The TM is instead the monitoring function, i.e., the retrieval of the whole recordings and status of the spacecraft. This information is downloaded to the ground through a space-to-Earth link and then redirected to the MOC. Depending on the number and size of the spacecraft subsystems, TM data rates can range from kbps to Mbps. Finally, tracking is a function that aids the determination of the spacecraft's flight dynamics. Namely, an RNG signal is sent from the TT&C ground station to the spacecraft that, in turn, transposes it back to the ground (i.e., it does a *RNG turn-around*). In this way, the TT&C ground station can estimate the round-trip time and thus

<sup>1</sup>Andrea Modenini is with the European Space Agency at European Space Research and Technology Centre (ESA/ESTEC), 2201AZ Noordwijk, The Netherlands (email: andrea.modenini@esa.int).

<sup>2</sup>Barbara Ripani is with Politecnico di Torino, Department of Electronics and Telecommunications (DET), I-10129 Torino, Italy (email: barbara.ripani@polito.it).

The view expressed herein can in no way be taken to reflect the official opinion of the European Space Agency.

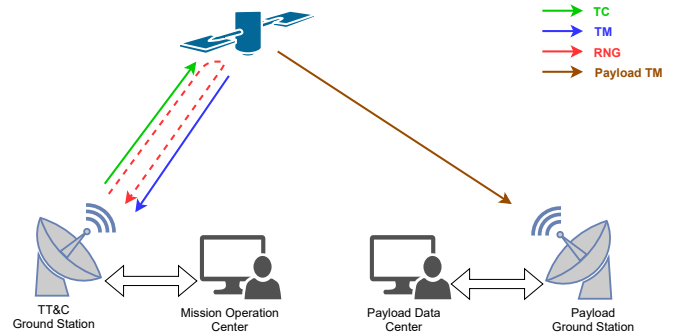


Figure 1. Sketch of the TT&C system: the ground segment can operate and monitor the spacecraft by means of the TC and TM links. The payload data can be instead retrieved by means of a dedicated payload TM link (if the TM link is not sufficient for performing such a function). The RNG is instead performed by means of a dedicated signal that is transposed back to the ground.

determine the spacecraft distance. Additionally, it can adopt the Doppler measure in the downlink to predict the spacecraft radial velocity w.r.t. the ground station. Theoretically, the just described TT&C links cover all directions for guaranteeing the mission data flow. However, spacecraft often embark a payload (e.g., scientific instruments) that produces a lot of information. Thus, the TM link could be inadequate for downloading such an amount of data. Hence, the TT&C is often complemented with a dedicated payload data transmission (PDT) link, from the spacecraft to a dedicated payload ground station that, in turn, redirects the received stream to the payload data center.

Clearly, the TT&C is a critical element for the success of any space mission. However, whoever tries to review the available TT&C literature can quickly realize that the topic is a “niche field” and that getting familiar with this domain can be very complicated: only a small bunch of companies have TT&C expertise, and public material is rather limited, papers are usually quite advanced (clearly meant for those already expert in the field), and academic material is almost not existing.

Hence, the objective of this paper is to provide a TT&C tutorial by reviewing the general concepts and state-of-the-art. The authors wrote Section II and III to be comprehensible to any professional or student in the telecommunication field for understanding the TT&C basics. In the following sections, the paper goes more in-depth by providing mathematical formulas, tables, discussion about trade-offs, and a large set of references, easing the transition for the reader to more advanced papers. In support of the explanation, several examples will

be given, with particular reference to European technologies, standards, and European Space Agency (ESA) missions. Nevertheless, the here-provided content is also applicable to non-European space missions of major space agencies such as NASA, JAXA, and CNSA, since the standards and engineering described here are agreed upon at inter space-agency level.

On the other hand, this paper will not provide basics on general space engineering, such as satellite orbits, electromagnetic compatibility, space qualification, technology readiness, etc., although these are also relevant for TT&C engineering. In the authors' opinion, these topics are well covered by the existing literature and thus out of the objective of this paper. When these will be mentioned, references will be provided, and in case the reader is looking for an overview of space missions engineering, readings such as [1] and [2] are a good starting point.

The remainder of this tutorial is organized as follows: Section II provides a general overview of the TT&C subsystem, from the architecture to the main design drivers, complemented with a brief survey of actual TT&C subsystems. Then, Section III focuses on providing the basics about the physical layer of TT&C links, starting with an introduction to the modulation formats, and addressing the details of the three main links (TC, TM, and tracking) along with their sizing. Then, Section IV lays out the fundamentals of the TT&C subsystem "core unit": the transponder. Section V follows up, providing an overview of the most recent techniques (under research and development) that could be implemented in future TT&C systems. Section VI explains instead the overall standardization framework, highlighting the main applicable standards that are used in this field. Finally, Section VII draws the conclusions.

## II. THE TT&C SUBSYSTEM

The design of a TT&C subsystem is not a standard task. Different space mission objectives and requirements, or simple engineering choices, can lead to completely different configurations. However, as shown in this section, some commonalities in the TT&C design (and the rationale behind them) can be identified. This section will describe how a TT&C subsystem is organized, providing details on major design drivers such as frequency allocations and reliability. Then, these concepts will be re-emphasized by surveying the TT&C subsystem of actual ESA satellites.

### A. Architectures

Figure 2 shows the most basic architecture for a TT&C subsystem: it is composed of two TC receivers, two TM transmitters, two diplexers, and two low gain antennas (LGAs), all interconnected by means of a radio-frequency distribution network (RFDN). The use of two receivers and transmitters is due to redundancy reasons (later discussed in Section II-C). In most cases, both receivers are kept always ON along the mission, i.e., they are in *hot redundancy* configuration. Differently, only one transmitter is kept ON during transmission periods, while the other is adopted as a *cold redundancy*. The transmitter and receiver are rarely embarked as separated

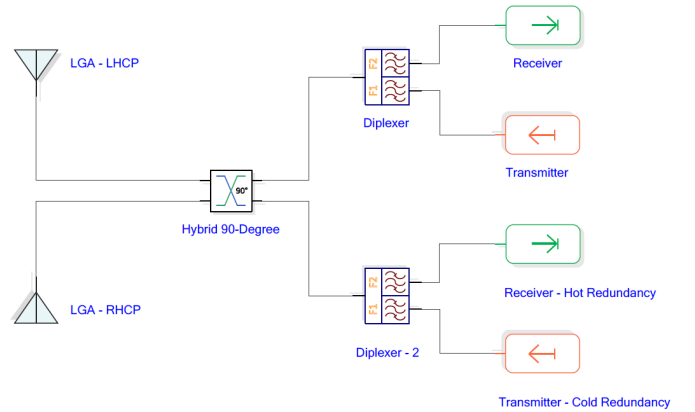


Figure 2. Block diagram of the basic TT&C subsystem architecture.

units: the two modules are typically integrated into a single unit that also performs the RNG turn-around and is known in "TT&C lingo" as *transponder*. Since TC and TM links work on different frequencies (later described in Section II-B), diplexers are adopted for de-multiplexing the two links from/to the transponder output and input. The diplexer can be either embarked as a separated unit or directly integrated as part of the transponder. The LGAs usually have wide coverage (possibly providing a gain  $\geq 0$  dB in about  $\pm 90$  degrees from boresight) and adopt opposite circular polarizations, namely, the left and right-hand circular polarization (LHCP and RHCP). Finally, the RFDN is the interconnection between all the aforementioned units and is the ensemble of cables, switches, hybrids, etc. In the example of Figure 2, the RFDN is composed of a 3 dB hybrid that interconnects with coaxial cables the diplexer ports with the two LGAs.

It is easy to see that this TT&C subsystem configuration strives to achieve very high reliability: it allows the spacecraft to receive TCs and transmit TM, regardless of the spacecraft's attitude, throughout all the mission phases. In fact, using two LGAs, it achieves an (almost) omni-directional coverage. Moreover, adopting LHCP and RHCP, it ensures that a signal received on a polarization will not cause destructive interference at the input of the receiver (as combinations of the same signal received by both the LGAs). Additionally, the signal transmitted by one of the two transmitters will always excite both antennas, while the signal received by any antenna will be seen at both receiver inputs. Finally, the redundant configuration allows the subsystem to be tolerant to anomalies/malfunctions of one transponder without causing the failure of the whole space mission.

A different approach is usually adopted for the PDT subsystems. The PDT subsystem basic architecture is shown in Figure 3. It is composed of two transmitters in a cold redundancy configuration, while the RFDN interconnects both transmitters to a medium/high gain antenna (MGA/HGA). The figure shows the example of an RFDN composed of a switch with coaxial cables.

The adoption of this configuration is driven by the need of achieving higher bit rates than those achievable by the TT&C subsystem when the spacecraft is in nominal conditions. Since

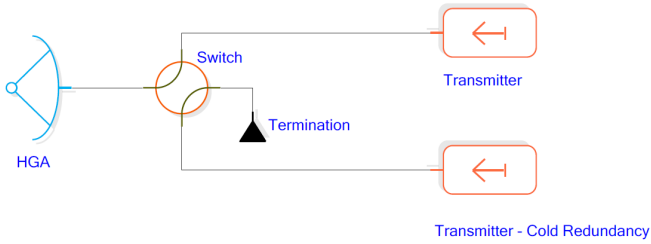


Figure 3. Block diagram of the basic PDT subsystem architecture.

the higher the bit rate, the higher the equivalent isotropically radiated power (EIRP), the PDT subsystem privileges the use of a switch (rather than a 3 dB hybrid) and an MGA/HGA (instead of LGAs). Even in case of failure of one transmitter, the MOC can activate the redundant transmitter chain through dedicated TC to the TT&C.

TT&C and PDT subsystems shall not necessarily be treated as two subsystems. When feasible, it is common to integrate the PDT transmitter into the TT&C transponder, and a common RFDN is adopted as interconnection with the antennas (LGAs and MGA/HGA). This will be better explained and shown with examples later provided in this paper.

### B. Frequency allocations

One of the main design drivers for the TT&C and PDT subsystems is the selection of the frequency allocations.

The Radio Regulations of the International Telecommunication Union (ITU/RR, [3]) define the frequency allocations that can be adopted depending on the radio communication service. Most of the TT&C systems usually fall under one of the following services:

- *Earth Exploration Satellite Service (EESS)*, that includes Earth Observation (EO) missions (performing meteorological measurements and global monitoring, like *Sentinels* [4]) or space missions that provide information regarding the characteristics of the Earth (like *Smile* mission [5]);
- *Space Research Service (SRS)*: applicable to space missions having scientific or technological research purposes. For this service there is a further distinction between *near Earth* missions and *deep space*, i.e., with distance from Earth less than 2 million of km (like *Euclid* or *Ariel*, [6]), or further (like the well-known *Rosetta* mission, or the novel *Solar Orbiter* [7]);
- *Space Operations Service (SOS)*: applicable to space missions that exclusively foresee the operation of the spacecraft, i.e., basic TC and TM (e.g., in-orbit servicing vehicles [8]).

Tables I and II provide a summary of the most used frequency allocations for designing Earth-to-Space (TC) and Space-to-Earth (TM) links, namely, S-, X-, K-, and Ka-Band<sup>1</sup>.

<sup>1</sup>It is pointed out that the nomenclature K- and Ka-Band is not uniform among the engineering domains. In this paper, it is adopted the most common naming used in ESA space missions, i.e., K-Band for  $\sim 27$  GHz links, and Ka-Band for  $\sim 32$  GHz links.

The TT&C engineer, when designing the subsystem, has to decide which frequency allocations select for all the possible TT&C and PDT links. This shall be done by taking into account major factors such as technology availability and maturity (identified by the so-called TRL [9], [10]), available ground station, and limitations from radio regulations.

At the time of writing, S-Band is the most adopted allocation for TT&C links: it relies on an extensive heritage and, also thanks to the large number of existing ground stations, it often results as the best choice for low-Earth orbit missions. However, its popularity is causing non-negligible problems in performing the frequency assignments for future missions, especially those that require large bandwidths. In particular, the 2200-2290 MHz band is one of the most densely occupied bands, and ESA missions use (and impose in their requirements) a maximum frequency assignment of 6 MHz [11].

X-Band for SRS (near Earth and deep space) is often selected as a baseline for the TT&C of Science missions, particularly those at Lagrange points or interplanetary missions. The technology development of X-Band units is well mature, and X-Band links are supported by space agencies' ground segment (e.g., the NASA DSN and ESA ESTRACK, [12], [13]). Since Science missions can have a PDT bit rate of about 1-10 Mbps, their PDT subsystem often adopts X-Band. Because of its popularity, similarly to S-Band, ITU imposes for X-Band near Earth a maximum frequency assignment equal to 10 MHz [11].

X-Band for EESS is often selected for PDT links of EO missions. Namely, its large bandwidth allows a bit rate as high as  $\sim 500$  Mbps. From Tables I and II, the reader can notice that X-Band for EESS could be adopted also for TT&C links, i.e., the TC link in 7190-7250 MHz and TM link in 8025-8400 MHz. However, at the time of writing, this design has never been adopted yet: the 7190-7250 MHz was opened up for EESS only in 2015 [14], and the technology is still under development.

K-Band will be widely adopted soon as an alternative to X-Band for both SRS and EESS missions. Namely, several EO missions will have PDT bit rates in the order of Gbps, while future Science missions forecast tens/hundreds of Mbps. Since these values cannot fit the X-Band allocations, K-Band PDT subsystems will be implemented.

Finally, Ka-Band is relevant for Deep Space missions. It is selected mainly for two functions: PDT (when bit rates do not fit the available X-Band) and for performing radio-science experiments, i.e., RNG measurements that provide specific information about planets gravity, atmosphere, etc., w.r.t. doing RNG in X-Band only. In light of these, Table III summarizes the most common frequency selection choices.

It shall be highlighted that ITU often does not define frequency allocations for all possible space missions, in particular Lunar and Martian, because of its primary interest in Earth RF interference. This task is covered by the *space frequency coordination group* resolutions and recommendations (SFCG [15], later explained in Section VI-C). Namely, for TT&C systems for Lunar missions, SFCG REC 32-2 applies, while for Martian missions SFCG REC 22-1 applies. These

Table I  
FREQUENCY ALLOCATIONS THAT CAN BE ADOPTED FOR  
EARTH-TO-SPACE TT&C LINKS.

Name	Allocation	Services
S-Band	2025-2110 MHz	SRS (near Earth), SOS, EESS
	2110-2120 MHz	SRS (deep space)
X-Band	7130-7190 MHz	SRS (deep space)
	7190-7235 MHz	SRS (near Earth)
	7190-7250 MHz	EESS

Table II  
FREQUENCY ALLOCATIONS THAT CAN BE ADOPTED FOR  
SPACE-TO-EARTH TT&C LINKS.

Name	Allocation	Services
S-Band	2200-2290 MHz	SRS (near Earth), SOS, EESS
	2290-2300 MHz	SRS (deep space)
X-Band	8025-8400 MHz	EESS
	8400-8450 MHz	SRS (deep space)
	8450-8500 MHz	SRS (near Earth)
K-Band	25.5-27.0 GHz	SRS (near Earth), EESS
Ka-Band	31.8-32.3 GHz	SRS (deep space)

recommendations provide the set of frequencies to be adopted depending on the link direction, such as from/to Earth, orbit-to-orbit, surface-to-orbit, and orbit-to-surface. For the detailed and latest version of the tables, the reader is referred to Table I provided in REC 32-2 and 21-1 on the SFCG website [15].

### C. Reliability and redundancies

The use of redundancies plays a fundamental role in the reliability of the spacecraft and the whole mission. It is standard to have a backup for any active unit of the subsystem. On the other hand, there are also missions in which no redundancy is adopted or required. For instance, Cubesats can accept a higher risk of failure, and their mission duration can be less than one year. Thus, the redundancy may burden the whole system (by increasing mass and power consumption) rather than benefit. To evaluate this trade-off, the *system reliability and single point failure analysis* is normally carried out throughout the project. Although engineers with dedicated expertise carry out this analysis, the TT&C engineer should be able at least to perform a preliminary assessment to understand whether redundancy is required or not. Thus, the objective of

Table III  
TYPICAL FREQUENCY ALLOCATION CHOICES FOR EACH KIND OF SPACE  
MISSION.

Mission type	TT&C	PDT
Earth Observation	S-Band	X-Band, if ~500 Mbps K-Band otherwise
Science (near Earth)	X-Band	as part of TT&C subsystem, if <10 Mbps dedicated K-Band subsystem otherwise
Science (deep space)	X-Band	as part of TT&C subsystem, or dedicated Ka-Band subsystem (if there are radio-science experiments needs)
Space Operations	S-Band	N/A

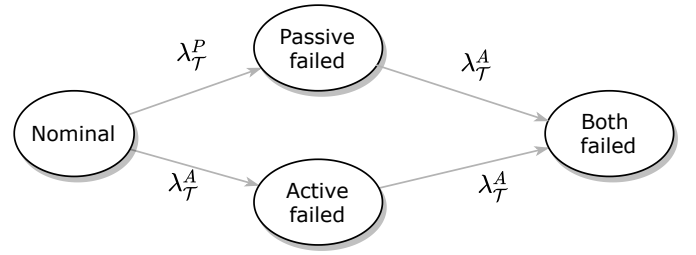


Figure 4. Continuous-time Markov chain describing the status of the transponder redundancy scheme of Fig. 2.

this section is to provide the basics of reliability analysis for the TT&C subsystems.

The lifetime of a generic unit  $u$  is modeled by means of an exponential random variable. This gives the probability of non-failure within the time  $t$  as

$$P_u(t) = e^{-\lambda_u t}, \quad (1)$$

where  $\lambda_u$  is the average number of failures in time, and thus  $1/\lambda_u$  is the average unit lifetime. The factor  $\lambda_u$  is often provided as the number of failures per  $10^9$  hours (with a unit known as *failure in time*, [FIT]), and it is computed based on the reliability information of the components which constitute the unit. Since the units have usually different operational modes, with different component derating values [16], the factor  $\lambda_u$  shall be computed as a weighted average among the modes. A common approach for active units is to define the average number of failures in time when the unit is ON ( $\lambda_{u,ON}$ ) and OFF ( $\lambda_{u,OFF}$ ), and thus the effective failure rate of the unit reads

$$\lambda_u = \lambda_{u,ON}d_{ON} + \lambda_{u,OFF}(1 - d_{ON}), \quad (2)$$

where  $d_{ON} \in [0, 1]$  is the unit duty cycle.

When redundancy comes into play, the problem becomes more complex. For the sake of clarity, we will refer to the TT&C subsystem example of Figure 2, where there is a redundancy scheme of two transponders (each including one transmitter, one receiver, and one diplexer). However, the concepts here presented can be easily generalized. The transponders have two possible modes: one mode with receiver and transmitter both ON, and the other one with the transmitter OFF. Hence, we can define the corresponding failure rates as  $\lambda_{T,ON}$ , and  $\lambda_{T,OFF}$  respectively. In turn, the two transponders can be adopted with different duty cycles. One transponder is adopted as an active transponder, i.e., transmitting when required, while the other as a passive (redundant) transponder, receiving only. Using Equation (2), the effective failure rates for the active and the passive transponder are

$$\begin{aligned} \lambda_T^A &= \lambda_{T,ON}d_{ON} + \lambda_{T,OFF}(1 - d_{ON}), \\ \lambda_T^P &= \lambda_{T,OFF}. \end{aligned}$$

We can now describe the transponder redundancy scheme by means of a continuous-time Markov chain [17] as the one shown in Figure 4. This Markov chain has the following states:

- *nominal*, when both transponders are functional. One transponder is used as the active unit, while the other one as the passive one;

- *active failed*, when the active transponder has failed. Thus the passive transponder is activated;
- *passive failed*, when the passive transponder has failed. The active transponder stays as it is;
- *both failed*. Thus, the whole redundancy scheme has failed.

The corresponding Markov chain rate matrix is equal to

$$\mathbf{R} = \begin{bmatrix} -\lambda_{\mathcal{T}}^A - \lambda_{\mathcal{T}}^P & \lambda_{\mathcal{T}}^A & \lambda_{\mathcal{T}}^P & 0 \\ 0 & -\lambda_{\mathcal{T}}^A & 0 & \lambda_{\mathcal{T}}^A \\ 0 & 0 & -\lambda_{\mathcal{T}}^A & \lambda_{\mathcal{T}}^A \\ 0 & 0 & 0 & 0 \end{bmatrix}. \quad (3)$$

Since the redundancy scheme fails when the Markov chain ends in the final state, the probability that this happens during the time  $t$  can be computed by means of the Kolmogorov forward equation [17]. The solution of the equation (after some calculations) provides that the reliability  $P_{\mathcal{T}2}(t)$  of the two transponders is

$$\begin{aligned} P_{\mathcal{T}2}(t) &= 1 - [e^{\mathbf{R}t}]_{1,4}, \\ &= e^{-\lambda_{\mathcal{T}}^A t} \left[ 1 + \frac{\lambda_{\mathcal{T}}^A}{\lambda_{\mathcal{T}}^P} (1 - e^{-\lambda_{\mathcal{T}}^P t}) \right], \end{aligned} \quad (4)$$

where  $e$  denotes the matrix exponential, and  $[\cdot]_{1,4}$  the entries of the matrix in position (1,4). We are now ready to compute the reliability of the full TT&C subsystem  $P_{\text{TT\&C}}(t)$ . Since all other units do not adopt any redundancy, the reliability is simply given by

$$P_{\text{TT\&C}}(t) = P_{\mathcal{T}2}(t)P_{\text{RFDN}}(t)P_{\text{LGA}}^2(t), \quad (5)$$

where  $P_{\text{RFDN}}(t)$  and  $P_{\text{LGA}}(t)$  have expression as shown in (1). The equation above is often reported in the reliability analysis report by means of a block diagram as the one shown in Figure 5, which represents redundant units as parallel blocks, and non-redundant ones as serial blocks. Once the  $\lambda_u$  values are defined, Equation (5) can be easily evaluated as a function of time. Typical values for the transponder failure rate are  $\lambda_{\mathcal{T},\text{ON}} \sim 1000 - 1500$  and  $\lambda_{\mathcal{T},\text{OFF}} \sim 500 - 750$  FIT, while for passive units can be less than 20 FIT.

Figure 6 shows the plot of (5) as function of the time, by using  $\lambda_{\mathcal{T},\text{ON}} = 1500$ ,  $\lambda_{\mathcal{T},\text{OFF}} = 500$ ,  $d_{\text{ON}} = 1$ ,  $\lambda_{\text{LGA}} = 14$ , and  $\lambda_{\text{RFDN}} = 1.55$ . For comparison, the figure also shows the reliability in the absence of transponder redundancy, and a typical system requirement of 99% reliability. As expected, the use of the redundancy, especially for active units, has a major impact. In the example, the subsystem with transponder redundancy has a reliability of 99% up to  $\sim 8.5$  years. On the other hand, a single transponder could suffice only for missions lasting less than 1 year.

The mathematical framework here presented can be easily generalized to complex TT&C and PDT architectures (like those presented in the following section). In fact, for any set of redundant units, a Markov chain (and its rate matrix) can be defined, and the reliability can be computed numerically by means of Equation (4).

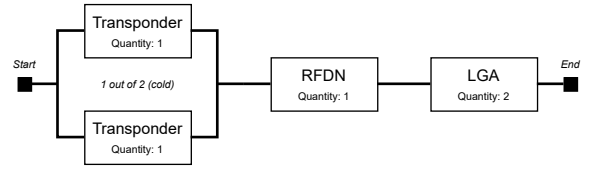


Figure 5. Reliability block diagram of the TT&C subsystem in Figure 2.

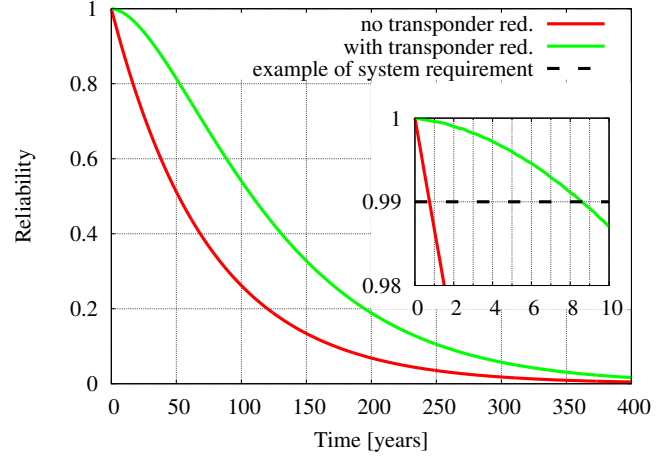


Figure 6. Reliability as function of the time for the TT&C subsystem in Figure 2.

#### D. Review of actual TT&C systems

As discussed, the TT&C subsystem design widely varies depending on several drivers (the kind of mission, bit rates, frequency regulations, reliability needs, etc.). This section shows some examples of actual subsystem architectures, highlighting the rationale behind their design and re-emphasizing the basics discussed in past sections.

Sentinel-1 ([4], [18]) is an EO satellite operating in Sun-synchronous orbit around Earth, with altitude  $\sim 690$  km. It has a TT&C subsystem in S-Band, able to achieve 64 kbps in TC and 2 Mbps in TM, and a PDT subsystem in X-Band (EESS), transmitting at 520 Mbps. The TT&C subsystem is composed of two (low-gain) *helix antennas* and two transponders with a diplexer each, exactly as the basic TT&C architecture in Figure 2. The two LGAs, as shown in Figure 7, are placed on opposite sides of the spacecraft: one faces the Earth direction (in the +Z spacecraft axis), and one the zenith (-Z axis). The LGAs have opposite circular polarization, thus providing an omni-directional coverage.

Instead, Figure 8 shows the Sentinel-1 PDT subsystem. It is an X-Band (EESS) subsystem able to downlink at 560 Mbps. Unfortunately, a single transmitter could not support such a bit rate. Thus, differently from the basic scheme of Figure 3, the TT&C subsystem was designed with two transmitting chains of 280 Mbps, each composed of a nominal transmitter, a redundant one, and traveling wave tube amplifiers (TWTAs) as external high power amplifiers. Then, the two transmitting chain signals are multiplexed by means of an output multiplex filter (OMUX). The PDT antenna is instead an *isoflux* [19]. It is mounted on the +Z spacecraft axis (see Figure 7) facing

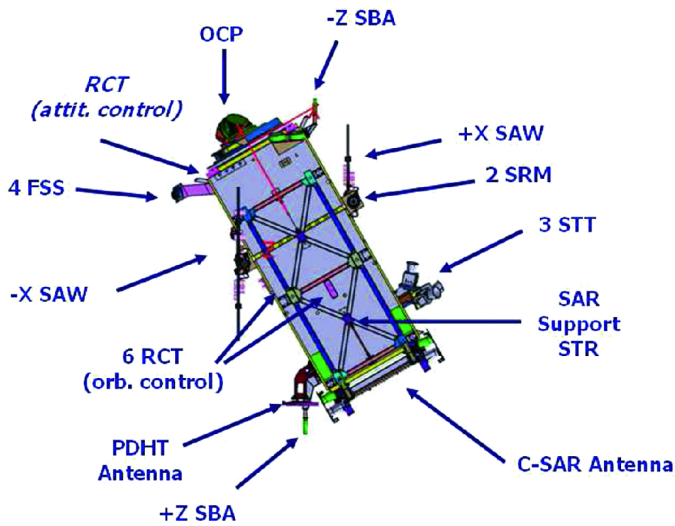


Figure 7. Platform configuration of Sentinel-1, showing the S-Band antennas (SBAs) and the X-Band PDT antenna (denoted in this figure as PDHT antenna). Image credit [20].

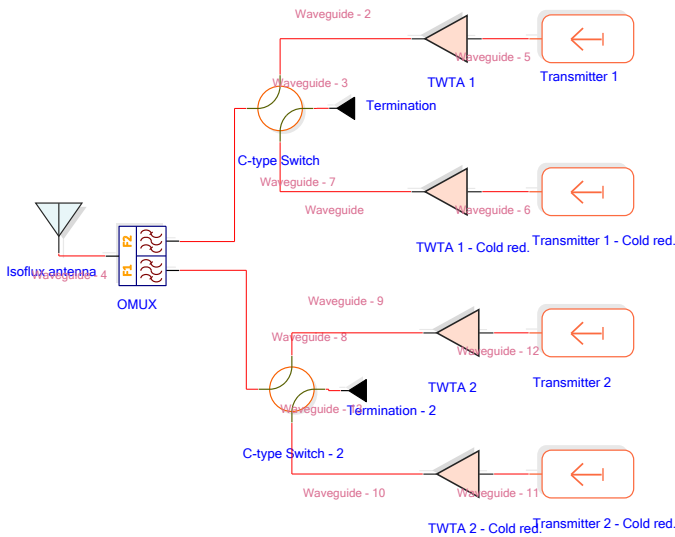


Figure 8. Block diagram of the PDT subsystem of Sentinel-1 (see [18]).

Earth, and it has a shaped beam that guarantees that the signal strength (as seen from Earth) remains almost constant, no matter what is the angle of view, and without the need of on-board steering of the antenna.

Euclid [21] is a near Earth Science mission that will operate in a large amplitude orbit around the second Sun-Earth Lagrange point (SEL2), with a distance from Earth up to ~1.8 million km. Euclid TT&C subsystem is in X-Band (SRS near Earth), able to support TC and TM links in the order of some kbps, and it has a block diagram, as shown in Figure 9. The TT&C subsystem adopts a scheme with transponder redundancy and two helix antennas, LGA-1 and LGA-2, with opposite polarizations. These were mounted as shown in Figure 10 for providing an (almost) omni-directional coverage. Differently from the basic TT&C subsystem architecture of Figure 2, a third antenna (LGA-3) was included: mounted on

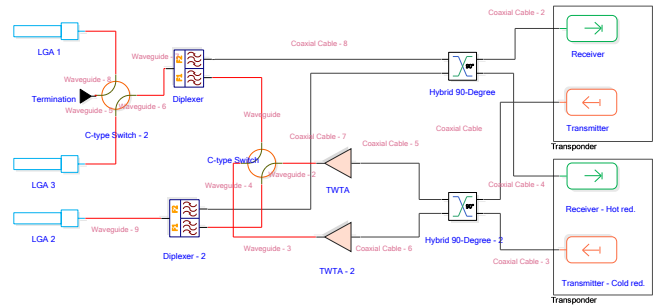


Figure 9. Block diagram of the TT&C subsystem of Euclid (see [21]).

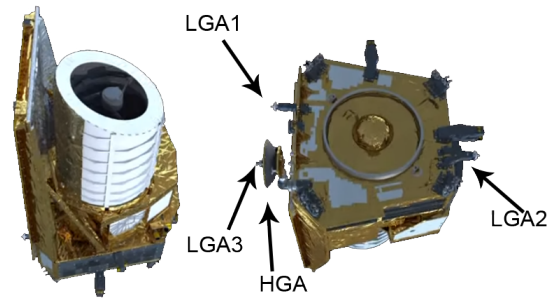


Figure 10. Euclid satellite configuration, as seen from above (left) and below (right), and showing the three X-Band LGAs and the K-Band HGA.

an antenna pointing mechanism (on top of the HGA, later explained) that always points to Earth during nominal phases. Hence, depending on C-type switch-2 position (as shown in the block diagram), the spacecraft can use the LGA-3 for having higher TC and TM bit rates during nominal phases, or LGA-1 and 2 when in need of an omni-directional pattern. For achieving the required EIRP, TWAs are adopted as external power amplifiers and interconnected to the diplexers by means of a second C-type switch that, in turn, provides a cross-strapping with all the LGAs. Finally, 3-dB hybrids are adopted for cross-strapping receivers and transmitters with the diplexers and TWAs, respectively. The Euclid PDT subsystem, shown in Figure 11, is instead composed of one HGA and two redundant transmitter chains. The only difference w.r.t. the basic PDT architecture of Figure 3 is the presence of TWAs that are cross-strapped with the transmitters by means of a 3 dB hybrid.

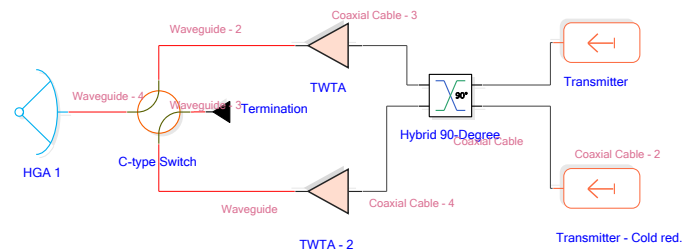


Figure 11. Block diagram of the PDT subsystem of Euclid (see [21]).

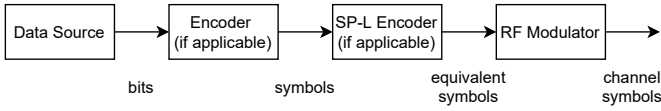


Figure 12. TT&C nomenclature for bits, symbols, equivalent symbols, and channel symbols.

### III. TT&C LINKS

After having discussed the TT&C from a subsystem perspective, this section aims to provide the basics of its physical layer. TT&C links are designed according to the standards dictated by the *consultative committee for space data systems* (CCSDS) and, for European missions (including ESA), also to those of the *European cooperation for space standardization* (ECSS), later described in Section VI. For the sake of clarity, since the standards are very similar, we will refer in the following sections to ECSS standards. However, the reader can find later some of the major differences between the two standards in Section VI-B.

It is also pointed out that the classical TT&C nomenclature shown in Figure 12 is adopted. The word *bit* means the useful unit of information while *symbols* are the bits after encoding. In the case of SP-L modulation (later explained), rates are expressed in terms of *equivalent symbols* that are nothing else than half of a symbol. Finally, modulation symbols are denoted as *channel symbol*. While rates for bits are expressed with the classical *bps* unit, to complicate things, TT&C engineers usually adopt the symbol per second unit *sps* for symbols, equivalent symbols, and channel symbols. Hence, the reader is recommended to always pay special attention to the kind of symbols in question.

The remainder of this section is organized as follows. First, Section III-A describes the RF modulations adopted in TT&C and their spectral properties. Then, Sections III-B and III-C provide a detailed description of the physical layer for TC and TM, explaining how to use a specific modulation and coding format for each kind of satellite mission. Additionally, they include discussions about performance, advantages, and disadvantages. Sections III-D and III-E describe the waveform adopted for ranging links and how the ranging signal combines with TC and TM data communications. Finally, Section III-F defines the link sizing (the link budget) for satellite missions, showing a small example as a tutorial exercise.

#### A. RF modulations

In TT&C there are basically two families of RF modulations: *residual carrier* and *suppressed carrier* [22]. Suppressed carrier modulations are classical linear modulations as BPSK, QPSK, OQPSK, 8PSK, and amplitude PSK (APSK, [23]), for which group of bits/symbols are mapped into specific channel symbols. On top of these, the well-known GMSK modulation [24] can be also adopted. Being this kind of modulations well-known, they will not be treated in this paper. For further detail on the constellation formats, mapping, etc., adopted in TT&C, the reader can refer to [25], [26]. Differently, TT&C residual carrier modulations are not (anymore) much adopted

in other telecommunication fields, and thus special focus will be given in this section.

As the name suggests, a residual carrier modulation is a format that keeps a leftover of the carrier tone instead of using all available power for transmitting the information. The advantage of this old-fashioned signal is that the residual carrier acts as a “permanent pilot” that can be adopted for easy acquisition and synchronization, especially at low signal-to-noise ratios (SNRs). The complex base-band mathematical expression, normalized in power, of a residual carrier modulation is a phase modulation (PM) reading

$$s(t) = e^{jm_x x(t)}, \quad (6)$$

where  $m_x$  is the modulation index and  $x(t)$  is the modulating signal. In most of the ESA satellite missions, the modulating signal  $x(t)$  can be a binary non-return-to-zero signal with sub-carrier (NRZ/BPSK), or, split-level (SP-L).

The NRZ/BPSK signal reads

$$x(t) = \sum_k a_k p(t - kT) \sin(2\pi f_x t), \quad (7)$$

where  $T$  is the channel symbol time,  $p(t) = \text{rect}(t/T)$  is a rectangular shaping pulse,  $a_k \in \{\pm 1\}$  are binary channel symbols, and  $f_x$  is the sub-carrier frequency. Plugging (7) into (6), the transmitted signal reads

$$s(t) = e^{jm_x \sum_k a_k p(t - kT) \sin(2\pi f_x t)},$$

and thus a PM NRZ/BPSK signal (NRZ/BPSK/PM) is obtained. Although the full expression of the NRZ/BPSK/PM signal can appear cumbersome, it has a simple approximation. In fact, using the Jacobi-Anger identity [27],  $s(t)$  can be rewritten as

$$s(t) = \sum_i J_i \left( m_x \sum_k a_k p(t - kT) \right) e^{j2\pi i f_x t},$$

where  $J_i(\cdot)$  is the modified Bessel function of the first kind. Taking into account that  $J_i(m_x) \rightarrow 0$  for  $i \rightarrow \infty$ , it can be shown that the signal is well approximated by the expression

$$s(t) \approx J_0(m_x) + 2jJ_1(m_x) \sum_k a_k p(t - kT) \sin(2\pi f_x t). \quad (8)$$

From this equation it can be observed that  $s(t)$  is composed by a residual carrier that keeps a fraction equal to  $J_0(m_x)^2$  of the total signal power, while only  $2J_1(m_x)^2$  is adopted for the transmitting data over the sub-carrier.

Differently, a SP-L signal reads

$$x(t) = \sum_k a_k p(t - kT), \quad (9)$$

where  $p(t) = \text{rect}((2t - T/2)/T) - \text{rect}((2t + T/2)/T)$  is a Manchester encoded shaping pulse. Since Manchester encoding has two rising edges per symbol time  $T$ , the equivalent symbol time (as explained in Figure 12) is equal to  $T/2$ . Plugging (9) into (6), a PM SP-L signal (SP-L/PM) is obtained and, by using Euler’s formula, it reads

$$s(t) = \cos(m_x) + j \sin(m_x) \sum_k a_k p(t - kT). \quad (10)$$

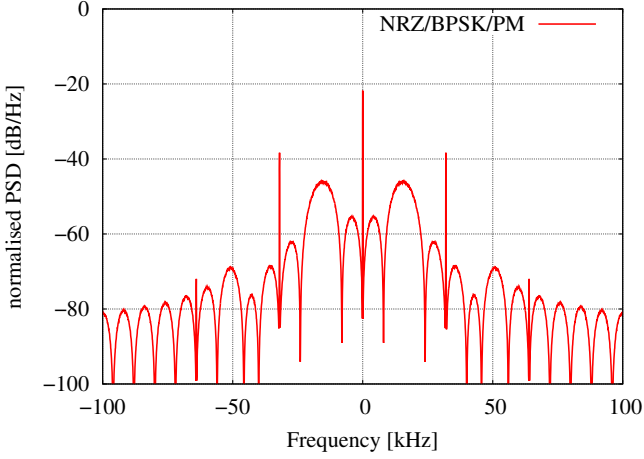


Figure 13. Normalized PSD for a NRZ/BPSK/PM signal, modulation index  $m_x = 1.0$  rad/peak, channel symbol rate  $1/T = 8$  ksp/s, and sub-carrier frequency  $f_x = 16$  kHz.

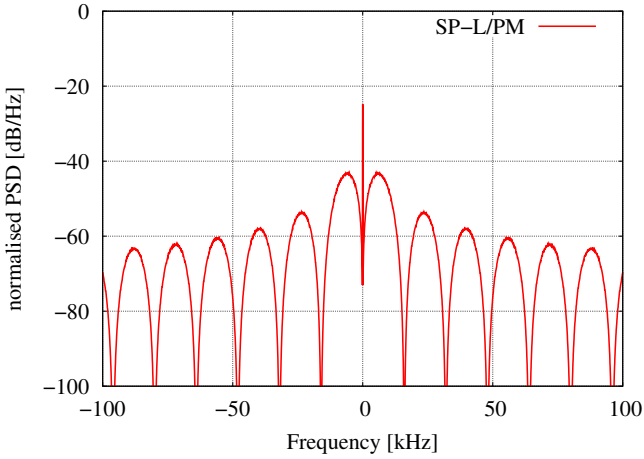


Figure 14. Normalized PSD for a SP-L/PM signal, modulation index  $m_x = 1.0$  rad/peak, and channel symbol rate  $1/T = 8$  ksp/s.

From the equation, it is easy to see that the SP-L/PM signal has a residual carrier with power fraction equal to  $\cos(m_x)^2$ , while only  $\sin(m_x)^2$  is used for data transmission.

Figures 13 and 14 show the simulated spectra of a NRZ/BPSK/PM and of a SP-L/PM signal, with a resolution bandwidth  $R_{BW}$  of 58.6 Hz. Both signals have modulation index  $m_x = 1.0$  rad/peak and channel symbol rate  $1/T$  equal to 8 ksp/s. In the case of NRZ/BPSK/PM signal a sub-carrier with  $f_x = 16$  kHz was adopted. In agreement with the mathematical equations derived in (8) and (10), we can see that the residual carrier has normalized power spectral density (PSD) equal to  $J_0(m_x)^2/R_{BW}$  and  $\cos(m_x)^2/R_{BW}$ , respectively. Additionally, we can observe that the main lobes (corresponding to the information signal), in the case of NRZ/BPSK/PM, are at  $f_x = \pm 16$  kHz, while for SP-L/PM are centered at about  $1/T = \pm 8$  kHz. By means of (8) and (10), it can be shown that the normalized PSD for these lobes is equal to  $TJ_1(m_x)^2$  and (about)  $T \sin(m_x)^2/2$ .

RF modulations have several requirements to be compliant,

dictated by both the CCSDS and ECSS. These can refer to maximum occupied bandwidth, spectral masks, maximum power flux density on Earth's surface, modulation linearity, frequency stability, and many others that cannot be stated by means of an exhaustive list, also because they can be tailored depending on specific mission needs. For an effective requirement coverage (but not complete), the reader can refer to the ECSS standard in [11].

### B. TC links

TC links for space missions are usually designed in compliance with the requirements dictated by the ECSS with modulation, synchronization, and channel coding as provided in [11], [28].

The TC shall be a reliable and low data rate link for ensuring the spacecraft always execute the commands sent from ground. Thus, according to these standards, the TC physical layer adopts residual carrier modulations and a discrete set of symbol rates. Namely, the TC link can have a symbol rate multiple or sub-multiple of 4000 sp/s with respect to a factor of  $2^n$ . The minimum and maximum rates are 7.8125 sp/s and 256 ksp/s, respectively. Additionally, depending on the chosen symbol rate, the TC modulation has to comply with the cases reported in Table IV: for rates between 7.8125 and 4000 sp/s, the TC signal shall be NRZ/BPSK/PM, while SP-L/PM otherwise. Further, the NRZ/BPSK/PM shall have a sinusoidal sub-carrier having frequency  $f_x$  equal to 8 or 16 kHz, and a modulation index ranging from 0.2 to 1.4 rad/peak. Differently, for SP-L/PM, no sub-carrier shall be adopted, and the modulation index shall be between 0.2 and 1.0 rad/peak.

The TC coding and synchronization layer foresees the use of a Bose–Chaudhuri–Hocquenghem (BCH) code [29] or low-density parity-check code (LDPC) [30]. For the sake of clarity, in this section, we limit the discussion to the BCH case, which was the only possible coding scheme for satellite missions till 2021, while LDPC will be discussed in Section V. The BCH for TC, usually denoted as BCH(63,56), encodes 56 bits into a codeword of 63 bits, plus an additional 0 bit as filling (thus making a total codeword length of 64 bits). The full specification of this code and its encoding procedure can be found in [31]. However, it is important to highlight that the BCH in question can be either adopted in a triple-error detection (TED) mode or in a double-error detection mode with single error correction (SEC). ECSS in [28] recommends to use the latter only. As shown in Figure 15, the TC frame (coming from the data link layer [32]) is sliced into blocks of 56 bits<sup>2</sup> and randomized by means of an XOR with a specific pseudo-random sequence defined by the standard. These blocks are then BCH encoded into a 64-bit codeword, finally forming a BCH *codeblock*<sup>3</sup>. At last, a *communication link transmission unit* (CLTU) is constructed by adding a 16-bits start sequence and a 64-bits tail sequence. The start sequence, expressed in hexadecimal, reads 0xEB90: this specific bit pattern has good

<sup>2</sup>In case the TC frame is not a multiple of 56 bits, then a *filling* is performed by appending the sequence 0101... to the TC frame until the TC frame has the number of bits required.

<sup>3</sup>For the reader's convenience, it is pointed out that, in this paper, we refer to a codeblock as a group of codewords.

Table IV  
TC SYMBOL RATES, MODULATIONS (WITH USE OF SUB-CARRIERS), AND ENCODING, ACCORDING TO ECSS STANDARDS.

Symbol rate	Modulation	Sub-carrier $f_x$	Sub-carrier waveform	Modulation index $m_x$	Encoding
$4000 / 2^n$ $n = 0, \dots, 9$	NRZ/PSK/PM	8 or 16 kHz	$\sin(\cdot)$	0.2 - 1.4 rad/peak	BCH or LDPC
$4000 \cdot 2^n$ $n = 1, \dots, 6$	SP-L/PM	N/A	N/A	0.2 - 1.0 rad/peak	BCH or LDPC

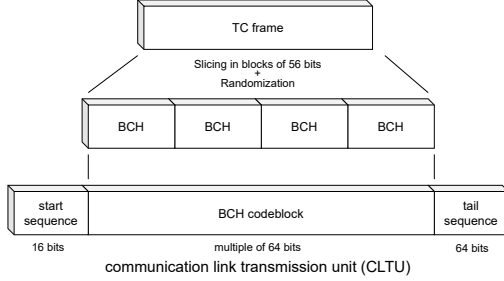


Figure 15. Encapsulation of a TC frame into a CLTU.

autocorrelation properties that allow to synchronize the start of a CLTU and delimit the beginning of the first codeword. Differently, the tail sequence reads  $0xC5C5\dots C579$ , and it is a specific pattern constructed to be *non-correctable*<sup>4</sup> by the BCH(63,56) decoder (with a rationale later explained).

The CLTUs' transmission follows a specific procedure, known as *physical layer operation procedure 2* (PLOP-2)<sup>5</sup>, based on a specific receiving logic: namely, the TC receiver shall be designed by implementing the state diagram shown in Figure 16. According to the figure, the receiver starts from an *Inactive* state, waiting for detecting a bit stream and achieving the bit lock ( $E1$  event). Following the event, the receiver moves into a *search* state that looks for the CLTU starting sequence ( $E3$ ) that, once found, allows to initiate the decoding. During decoding, when non-correctable errors are found ( $E4$ ), the receiver goes back to the search state. In case the link is lost at any time (event  $E2$ ), the receiver returns to the inactive state. In light of this reception logic, PLOP-2 follows the process in Figure 17. The TC session is initiated by means of an unmodulated carrier followed by a TC signal with a 128-bit acquisition sequence (to not be confused with the CLTU start sequence) of an alternating bit 1 and 0, thus making the receiver move into the search state. At this stage, CLTUs are transmitted, each separated with an 8-bit idle sequence of an alternating bit 1 and 0. At the end of each CLTU, the tail sequence forces the BCH decoder at the receiving end to reject the codeword (event  $E4$ ). Thus, for each transmitted CLTU, the receiver moves from a decode to a search state and vice-versa. Finally, at the end of the TC session (when there are no more CLTUs to be transmitted), the signal is removed by

<sup>4</sup>In this paper and in the TC standards, a non-correctable pattern is a sequence for which the decoder is able to declare uncorrected errors. This definition is valid for a BCH decoder either in TED or SEC mode.

<sup>5</sup>Beyond PLOP-2, TC standards foresee also the use of the former PLOP-1, that shall be adopted exclusively for legacy missions. The full description of PLOP-1 can be found in [28].

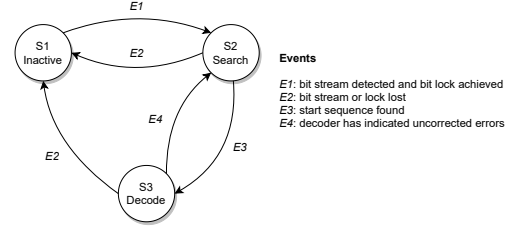


Figure 16. State diagram for the TC receiver.

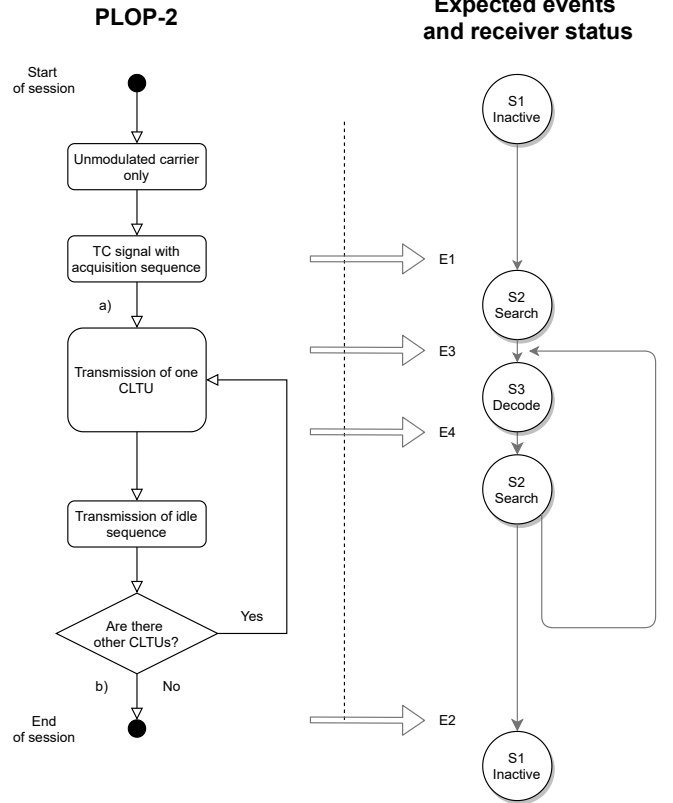


Figure 17. Flow diagram of PLOP-2 and expected events and receiver status for the correct reception of CLTUs during a TC session.

forcing the receiver to go back to the inactive state (event  $E2$ ). Optionally, at points a) and b) of Figure 17, a mission can consider introducing an idle sequence and an unmodulated carrier step, respectively.

As the reader may have noticed, the CLTU tail sequence is adopted as a non-correctable BCH codeword for finding the end of the CLTU itself. Consequently, standard bit or

synchronization errors can cause the CLTU to terminate prematurely, having the rejection of the full TC frame at the upper layer. Similarly, a missed error detection could cause undetected errors in the TC frame. We will now lay down the basics for estimating the probability of *TC frame rejection* and *undetected errors in a TC frame*. This will be done by considering the case of BCH(63,56) hard-decoding with SEC and assuming that the start sequence is accepted with a maximum of one error (as foreseen by ECSS [28]). For the complete mathematical details and the case of BCH hard-decoding with TED, the reader can refer to [33].

Since PLOP-2 starts with an unmodulated carrier and a 128-bit acquisition sequence (possibly extended by the idle sequence), the probability of missed bit detection and bit lock can be considered negligible. Thus, in practice, the main events that contribute to the incorrect CLTU rejection probability are: *start sequence not recognized*, *BCH codeblock rejected*, *tail sequence is missed*. The probability  $P_{\text{start}}$  that the start sequence is not recognized is trivially given by the probability that we get two or more errors in the 16-bit sequence. Namely,

$$P_{\text{start}} = 1 - (1 - P_b)^{16} - \binom{16}{1} P_b (1 - P_b)^{15}, \quad (11)$$

where  $P_b$  is the bit error rate. Differently, the probability  $P_{\text{BCH}}$  that a BCH codeblock is rejected can be quite cumbersome to compute. In fact, the codeblock is rejected if errors are detected in any of the BCH codewords. But, two or more errors (depending on their number and if they are even/odd) can still make the BCH decoder declare (mistakenly) the codeword valid. Luckily, these events are negligible in the overall probability calculation. Thus the probability  $P_{\text{BCH}}$  can be upper-bounded with good precision [33] as

$$P_{\text{BCH}} \leq 1 - \left[ (1 - P_b)^{63} + \binom{63}{1} P_b (1 - P_b)^{62} \right]^{N_{\text{BCH}}}, \quad (12)$$

where  $N_{\text{BCH}}$  is the number of BCH codewords per CLTU. Finally, the probability  $P_{\text{tail}}$  of missing the tail sequence is given by the probability that the tail sequence is a valid codeword. It can be shown that there are 1953 and 651 combinations of two and three errors, respectively, that contribute to such a probability, while other terms are negligible [33]. Consequently, the probability of missed tail sequence can be upper-bounded as

$$P_{\text{tail}} \leq 1953 \cdot P_b^2 (1 - P_b)^{61} + 651 \cdot P_b^3 (1 - P_b)^{60}. \quad (13)$$

We are now ready to compute the TC frame rejection rate and the probability of undetected errors. For the former, by considering that the CLTU contains a single TC frame, the probability of rejection  $P_{\text{TC, rej}}$  is given by (14). Namely, the frame is rejected if, in chronological order, the tail sequence of the previous CLTU is missed, the start sequence is not recognized, or the BCH codeblock is rejected. Similarly, using the approach of previous equations, the probability of undetected errors  $P_{\text{TC, und}}$  can be found: technical report [33] showed, by means of numerical simulations, that the main contributors to the undetected errors probability are 39060 and 9765 codewords of three and four errors, respectively. Thus,  $P_{\text{TC, und}}$  is well approximated by means of (15).

Figure 18 shows  $P_{\text{TC, rej}}$  and  $P_{\text{TC, und}}$  as functions of the energy-per-bit over noise spectral density  $E_b/N_0$  for the AWGN channel (for which it holds  $P_b = Q(\sqrt{2E_b/N_0})$ ). The probabilities are shown for  $N_{\text{BCH}}$  equal to 10 and 50. It can be seen that as  $N_{\text{BCH}}$  increases, the rejection and undetected errors probability (trivially) increase. This can be seen also in Figures 19 and 20, that show the probabilities as functions of  $N_{\text{BCH}}$  for different values of  $P_b$ . Consequently, if the mission imposes maximum values for  $P_{\text{TC, rej}}$  and  $P_{\text{TC, und}}$ ,  $P_b$  and  $N_{\text{BCH}}$  shall be sized properly.

As an example, let us consider  $P_{\text{TC, rej}} \leq 10^{-3}$  and  $P_{\text{TC, und}} \leq 10^{-9}$ , that are typical values for space missions [33]. Additionally, let us assume that  $P_b = 10^{-5}$ , as recommended by ECSS communication standard [34]. By considering such a  $P_b$ , we can see from the figures that the requirements are met as long as  $N_{\text{BCH}} \lesssim 50$ , while for larger codeblocks, we have  $P_{\text{TC, und}}$  that gets around  $10^{-8}$ . Thus, if  $N_{\text{BCH}} \geq 50$  is needed, then the designer has to decrease  $P_b$ .

In reality, space missions also have another alternative: TC frames can include a 16-bit cyclic redundancy check (CRC), as described in [35]. If the CRC is implemented  $P_{\text{TC, und}}$  decreases by several order of magnitude (e.g., from  $10^{-8}$  down to  $10^{-18}$ ), while  $P_{\text{TC, rej}}$  remains the same. This is done at the price of a small overhead in the TC frame and additional hardware complexity in the spacecraft receiving system. For further details, the reader can refer to [33], Section 9.5.

### C. TM links

TM links are designed in compliance with the requirements dictated by ECSS concerning modulation, synchronization, and channel coding, as provided in [11] and [36], respectively.

Table V shows a summary of the modulation schemes that can be adopted for the TM physical layer: it can be seen that the TM signal can be either a residual or a suppressed carrier modulation, depending on the target symbol rate and type of mission. Usually, low TM rates are meant for critical operations (e.g., a spacecraft in emergency mode), and thus residual carrier modulations are adopted. Differently, high rates are used for nominal operations and, since spectral efficiency is usually a concern, suppressed carrier modulations (possibly filtered) are adopted. In this respect, standards foresee that for rates below 60 kbps, an NRZ/PSK/PM can be adopted with a sinusoidal or squared sub-carrier depending if the mission is near Earth or deep space<sup>6</sup>. Differently, SP-L/PM can be used for rates between 10-1000 kbps. Although, based on the authors' personal experience, it is recommended to use a rate not higher than 128 kbps for easily meeting the bandwidth and spectral requirements previously mentioned in Section III-A. Finally, for any other data rate, suppressed carrier modulations, as reported in Table VI, can be adopted. However, the designer should take into account the following points:

- suppressed carrier modulations at low symbol rates (and thus operating at low SNR) can have synchronization

<sup>6</sup>The squared sub-carrier is obtained by replacing the term  $\sin(2\pi f_x t)$  in Equation (7) with  $\sum_k (-1)^k \text{rect}(2f_x t - k)$ , where  $\text{rect}(\cdot)$  a unitary squared pulse in  $[-0.5, 0.5]$ .

$$P_{TC,rej} \approx P_{tail} + (1 - P_{tail}) [P_{start} + (1 - P_{start}) P_{BCH}] \quad (14)$$

$$P_{TC,und} \approx 1 - [1 - 39060 \cdot P_b^3 (1 - P_b)^{60} - 9765 \cdot P_b^4 (1 - P_b)^{59}]^{N_{BCH}} \quad (15)$$

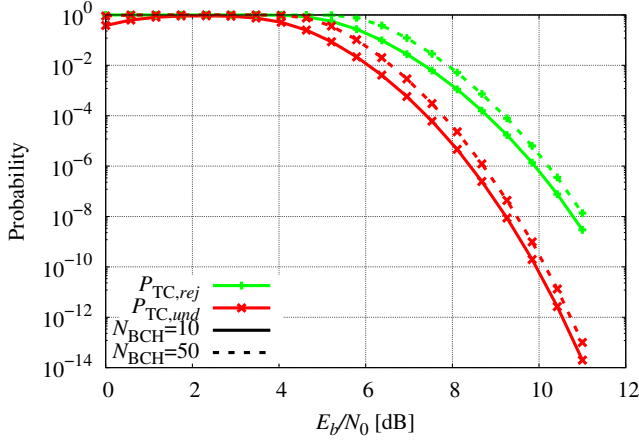


Figure 18. Probability of TC rejection rate  $P_{TC,rej}$  and of undetected errors  $P_{TC,und}$  as function of  $E_b/N_0$ .

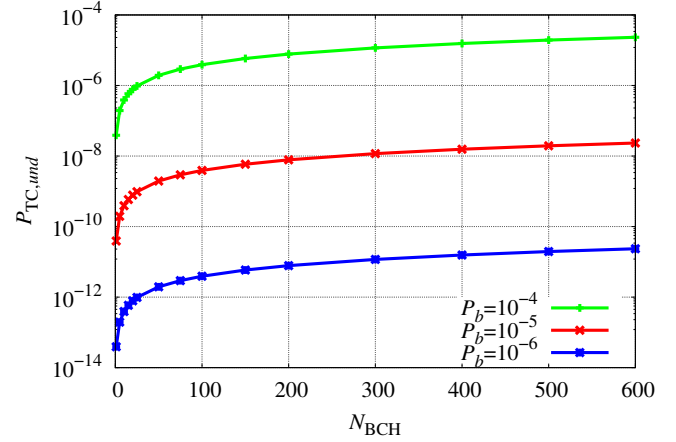


Figure 20. Probability of undetected errors  $P_{TC,und}$  in the CLTU as function of the number of BCH codewords per codeblock.

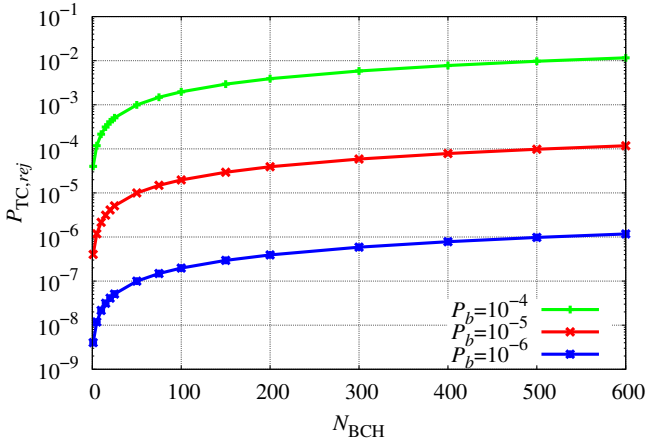


Figure 19. Probability of TC rejection rate  $P_{TC,rej}$  as function of the number of BCH codewords per codeblock.

issues. Hence, in the authors' experience, it is recommended to use suppressed carrier modulations only when the symbol rate is roughly higher than 1 Msps;

- Modulations as BPSK, QPSK, Unbalanced-QPSK (UQPSK), Offset-QPSK (OQPSK) are defined as direct modulation of a NRZ symbol stream (see [11], Section 6.2.3), hence with spectra resembling a  $\text{sinc}(\cdot)$ . Since these modulations are not spectrally efficient, ECSS [11] enforces to adopt them only for symbol rates  $\leq 2$  Msps for links in S- and X-Band, and  $\leq 20$  Msps for links in Ka-Band;
- Filtered OQPSK is obtained by using a squared-root raised cosine (SRRC) filter, having roll-off 0.5 or an elliptic filter. Similarly, TCM-8PSK, can adopt SRRC

with roll-off 0.35 or 0.5 or an elliptic filter;

- GMSK has a spectral efficiency driven by the parameter  $BT$ , i.e., the product of the one-sided 3-dB Gaussian filter bandwidth with the symbol time. This parameter shall be chosen as a trade-off between spectral efficiency and demodulation loss. Namely, as  $BT$  decreases, the spectral efficiency increases, but inter-symbol interference (ISI) at the receiver also increases. Differently, as  $BT$  increases, both spectral efficiency and ISI decrease. For this reason, it is recommended that near Earth missions, usually band-limited, implement GMSK with  $BT = 0.25$ . Differently, deep space missions, typically power limited, use GMSK with  $BT = 0.5$  [25];
- 8PSK trellis code modulation (8PSK-TCM) can be implemented either with a spectral efficiency factor (SEF) of 2 symbols/channel symbols, or, 2.5 symbols/channel symbols.

The TM synchronization and coding layer foresees the use of different coding schemes that can be applied at two different levels: at the TM transfer frame or *channel access data unit* (CADU) level (later defined). Table VII and VIII show the full list of coding techniques at these two levels, namely, Convolutional coding (CC, possibly punctured), Reed-Solomon (RS), Turbo codes, and LDPC. For the complete implementation details of these coding schemes, the reader can refer to the document [37].

TM frames can be encoded following two possible logic schemes: one specific for LDPC at the CADU level (as by Table VIII), and one adopted in all the other cases. The latter is shown in Figure 21. TM frames (coming from the data link layer [38]) are provided with an *attached synch marker* (ASM), a specific bit pattern that aids the frame

Table V  
TM SYMBOL RATES, MODULATIONS (WITH USE OF SUB-CARRIERS), AND ENCODING, ACCORDING TO ECSS STANDARDS.

Symbol rate	Modulation	Sub-carrier $f_x$	Sub-carrier waveform	Modulation index $m_x$	Encoding
0.1 – 60 ksps	NRZ/PSK/PM	2-300 kHz and multiple of symbol rate <sup>(*)</sup>	$\sin(\cdot)$ , if near Earth $\sum \text{rect}(\cdot)$ , if deep space	$\leq 1.5$ rad/peak, if near Earth $\leq 1.25$ rad/peak, if deep space	see Table VII
10 – 1000 ksps (recommended $\leq 128$ ksps)	SP-L/PM	N/A	N/A	$\leq 1.25$ rad/peak	see Table VII
any if filtered, limited to values in Table VI if unfiltered, (recommended $\geq 1$ Msps)	Suppressed carrier see Table VI	N/A	N/A	N/A	see Table VII

(\*) for sub-carrier frequency higher than 60 kHz, the frequency to symbol rate ratio shall not exceed 4 for near Earth missions, and 5 for deep space missions..

Table VI  
LIST OF ALLOWABLE TM SUPPRESSED CARRIER MODULATIONS.

Suppressed carrier modulation
BPSK <sup>(*)</sup>
QPSK <sup>(*)</sup>
UQPSK <sup>(*)</sup>
OQPSK <sup>(*)</sup>
Filtered OQPSK
GMSK
8PSK-TCM

(\*) only for symbol rates  $\leq 2$  Msps in S- and X-Band, and, for symbol rates  $\leq 20$  Msps in Ka-Band (as defined in Table II).

Table VII  
LIST OF ALLOWABLE TM CHANNEL CODES AT TM FRAME LEVEL.

Code	Rate
RS	223/255
RS (for 8PSK-TCM)	239/255
Turbo	1/6, 1/4, 1/3, 1/2
LDPC	1/2, 2/3, 4/5, 223/255 ( $\sim 7/8$ )

synchronization at the receiving end, and followed by the forward error correction (FEC) bits of one of the coding schemes in Table VII. The resulting frame, known as CADU, can be optionally randomized (except for its ASM) by means of an XOR with a specific pseudo-random sequence, as defined in [37]. In the only case of TM frames that are RS encoded or unencoded, then the stream of CADUs can be convolutionally encoded. The combination of RS with CC is known as *concatenated*.

Differently, when the LDPC in Table VIII is adopted, the logic scheme to be used is shown in Figure 22: a stream of synch-marked TM frames are asynchronously sliced into information blocks that, in turn, are LDPC encoded. Since the ASM cannot be employed anymore for frame synchronization,

Table VIII  
LIST OF ALLOWABLE TM CHANNEL CODES AT CADU LEVEL.

Code	Rate
CC	1/2
Punctured CC	2/3, 3/4, 5/6, 7/8
LDPC	1/2, 2/3, 4/5, 223/255 ( $\sim 7/8$ )

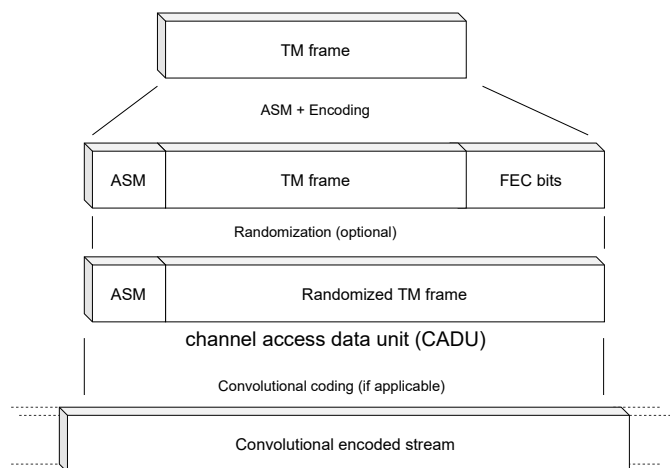


Figure 21. Encapsulation of a TM frame into a CADU. In case the TM frame is unencoded or RS encoded, it can be further protected with application of CC at CADU level.

the resulting LDPC codewords are grouped into blocks with attached a new marker, known as *code synch marker* (CSM). Each LDPC codeblock is composed by a (mission specific) fixed number of LDPC codewords. Consequently, for this case, the CADU is the composition of the CSM and the LDPC codeblock.

As the reader can notice, the TM link can be designed with different combinations of modulation and coding formats that have been expanding over time, following technical advances in the field, while keeping several technology features that justified their inclusion in the TM standards. However, in practice, missions resort only to a few cases. A summary of the most frequent design combinations, adopted in ESA missions, is shown in Table IX. In particular:

- EO missions typically have TT&C links with bit rates targeting 100-3000 ksps, thus resorting to SP-L/PM or OQPSK. These missions, because of their proximity to Earth, often have links with an SNR that is high enough to require only a moderate coding rate and gain. Thus, it is typical to adopt an RS or concatenated coding approach. Differently, their PDT usually targets hundreds of Mbps, taking the whole available bandwidth while maximizing as much as possible the spectral efficiency. For this

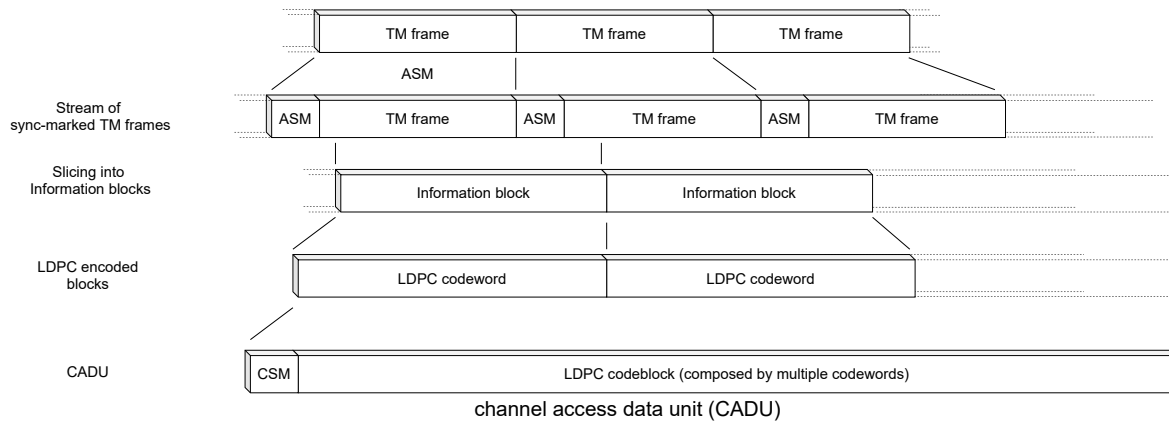


Figure 22. Encapsulation of TM frames into a CADU, when LDPC at CADU level is adopted: a stream of sync-marked TM frames is sliced into information blocks, that are then LDPC encoded. Finally, a multiple number of LDPC codewords are collected into a LDPC codeblock, and attached with the CSM.

Table IX  
COMMON DESIGN OF TM LINKS (MODULATION, CODING, AND  
FREQUENCY ALLOCATION) IN ESA MISSIONS.

Mission type	TT&C	PDT
Earth Observation	SP-L/PM or Filt. OQPSK RS only, or Concat. S-Band	8PSK-TCM RS (for 8PSK-TCM) X-Band
Science (near Earth)	NRZ/BPSK/PM or SP-L/PM CC, Concat. X-Band	GMSK ( $BT=0.25$ ) Punctured CC, Concat. X-Band
Science (deep space)	NRZ/BPSK/PM Turbo or LDPC X-Band	GMSK ( $BT=0.5$ ) Turbo or LDPC X-Band

reason, the EO PDT link can resort to 8PSK-TCM (with SEF equal to 2.5) combined with RS 239/255, thus with a total efficiency of about 2.3 bits per channel symbol;

- near Earth Science missions are often orbiting around Lagrange points, in particular SEL2, which is about 2 million km from Earth. Thus, the TT&C typically targets a few kbps for both TC and TM, and uses a residual carrier modulation with a moderate coding rate, like those of CC or concatenated. The PDT subsystem instead can target a few tens of Msps while being limited in bandwidth (see Section II-B). Thus, a combination of GMSK  $BT = 0.25$  with (possibly) punctured CC or concatenated is often a viable solution;
- Deep space missions, finally, are usually power limited. The TT&C cannot support more than a few kbps, and can target symbol rates as low as  $\sim 7.8$  sps. Similarly, the PDT symbol rate is usually in the order of some tens of kbps. Consequently, the use of low rate coding is often the best solution. Since bandwidth is not a concern, deep space missions can resort to resilient modulations as NRZ/BPSK/PM, GMSK  $BT = 0.5$ , or unfiltered suppressed carrier modulations.

#### D. Tracking

So far, the paper mostly dealt with the TC and TM functions. In this section, we will focus on the third fundamental function

of the TT&C subsystem: the tracking or, in other words, the measurement of satellite range and range rate.

Range measurements are carried out using a dedicated RNG signal sent from the ground station to the spacecraft and back to Earth (see Figure 1). Then, a distance measurement is derived by means of the round trip light time of the signal. For laying down the basics, let us consider, for a moment, a pure tone signal with frequency  $f_T$  transmitted from the ground station and received back with a phase difference  $\Delta\theta$ . An estimation of the spacecraft distance  $\hat{r}$  can be obtained as

$$\hat{r} = \frac{1}{2} \frac{\Delta\theta}{2\pi f_T} c,$$

where  $c$  is the speed of light. Although this kind of measurement is easy to implement, it has a major flaw: the selection of  $f_T$  is a trade-off between accuracy and ambiguity. Namely, at high frequency, the tone will complete several  $2\pi$  cycles in its round trip, causing the measurement to have an ambiguity equal to  $c/f_T$ . For instance, if the frequency tone is in the order of 100 kHz, the ambiguity will be in the order of thousand meters, way lower than the hundred/thousand kilometers usually required for orbit determination. On the other hand, at low frequency as 100 Hz, a small error as (say) 0.01 rad in the phase estimation, the measure will have a poor accuracy of about 2000 meters. To tackle this issue, different solutions can be adopted. A first solution is to use a multi-tone RNG signal which uses both high and low frequency tones. This was the rationale behind *code ranging*, defined in the ECSS standard [39]. The complex base-band mathematical expression of the code ranging signal reads

$$r(t) = e^{jm_r\Phi(t)}, \quad (16)$$

where  $\Phi(t)$  is the RNG signal, and  $m_r$  the modulation index. This signal, in turn, is a sub-carrier with frequency  $f_T$  (defined as the *fundamental tone*) and phase-modulated as

$$\Phi(t) = \sin(2\pi f_T t + m_T C_n(t)),$$

where  $m_T$  is the tone modulation index, and  $C_n(t)$  is a  $2^n$ -length code adopted for ambiguity resolution (being  $n$

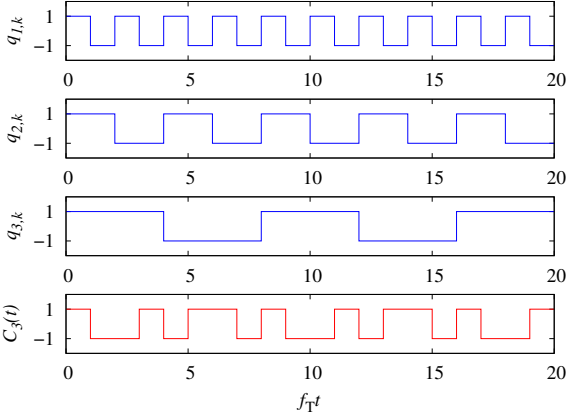


Figure 23. Plot of the 3-length code, obtained as composition of three tones with frequency  $f_T/2$ ,  $f_T/4$ , and  $f_T/8$ .

a design parameter). Namely,  $C_n(t)$  has expression

$$C_n(t) = \sum_k c_k \text{rect}(f_T t - k),$$

where  $c_k \in \{\pm 1\}$  belong to a  $2^n$ -length periodic sequence obtained as

$$c_k = q_{1,k} \cdot q_{2,k} \cdot q_{2,k} \cdots q_{n,k},$$

and  $q_{i,k} = (-1)^{\lfloor k/2^{i-1} \rfloor}$ .

Although the expression of the code ranging signal can appear quite cumbersome, it is nothing else than a tone of frequency  $f_T$ , phase modulated, with the introduction of lower frequencies by means of  $C_n(t)$ . In particular, if we adopt the Jacobi-Anger approximation (as done in Section III-A), the code ranging signal can be expressed as

$$r(t) \approx J_0(m_r) + 2jJ_1(m_r) \sin(2\pi f_T t + m_T C_n(t)), \quad (17)$$

that for  $n = 0$ , it holds  $C_0(t) = 1$ , and the signal is nonetheless than a residual carrier with power fraction equal to  $J_0(m_r)^2$ , and a tone with power fraction equal to  $2J_1(m_r)^2$ . These are complemented by tone replicas at multiple of  $f_T$  due to the higher-order terms of the Jacobi-Anger formula. Differently, for  $n > 0$ , the code  $C_n(t)$  introduces lower frequencies down to  $f_T/2^n$ . Figure 23 shows the example of the  $2^3$ -length  $C_3(t)$  (in red) and the analog equivalent of its sub-components  $q_{1,k}$ ,  $q_{2,k}$ ,  $q_{3,k}$  (in blue). It can be seen that the sub-components represent a square wave with frequency  $f_T/2$ ,  $f_T/4$ , and  $f_T/8$ , respectively, while the resulting signal  $C_3(t)$  is obtained as a combination of such waves.

The overall effect can be seen in Figure 24 and 25 that show the spectra for (16) with  $n = 0$  and  $n = 2$ , respectively, when the resolution bandwidth is  $R_{BW} = 4$  kHz. Both cases have modulation index  $m_r = 1.0$  rad/peak, frequency tone  $f_T = 448$  kHz, and (for  $n = 2$ ) a tone modulation index  $m_T$  equal to  $\pi/4$  rad/peak.

Beyond code ranging, there is a second solution that relies upon the same principle: the *pseudo noise ranging* (PN ranging). Namely, it adopts a ranging sequence that combines PN sequences, each characterized by a different period and thus

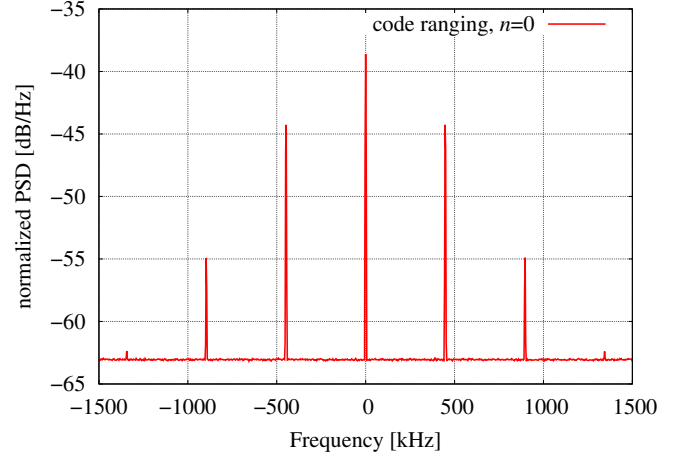


Figure 24. Normalized PSD for a code ranging signal,  $n = 0$ , frequency tone  $f_T = 448$  kHz, and modulation index  $m_r = 1.0$  rad/peak.

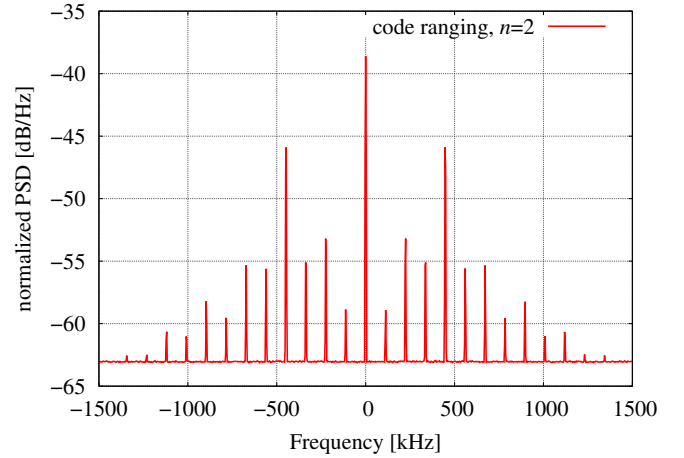


Figure 25. Normalized PSD for a code ranging signal,  $n = 2$ , frequency tone  $f_T = 448$  kHz, modulation index  $m_r = 1.0$  rad/peak, and tone modulation index  $m_T = \pi/4$  rad/peak.

different harmonics. This kind of waveform, standardized by the CCSDS [40], was introduced to cope with high position accuracy requirements of future space missions. For this reason, the standard foresees the possibility of implementing regenerative ranging [41] in low SNR scenarios or when high accuracy is demanded. As for the code ranging, the complex base-band signal can be written in the form reported in (16), where  $\Phi(t)$  is defined as

$$\Phi(t) = \sum_k c_k h(t - kT_c), \quad (18)$$

being  $T_c$  the chip time, and  $c_k \in \{\pm 1\}$  the chips belonging to the ranging sequence. Moreover, the chip pulse shape  $h(t)$  reads

$$h(t) = \begin{cases} \sin(\pi t/T_c) & t \in [0, T_c] \\ 0 & \text{elsewhere} \end{cases}.$$

The ranging chip sequence  $\{c_k\}$  is built-up as a weighted voting that reads

$$c_k = \text{sign}(\nu C_{1,k} + C_{2,k} - C_{3,k} - C_{4,k} + C_{5,k} - C_{6,k}),$$

where  $C_{1,k}, \dots, C_{6,k}$  are six periodic *component sequences* as reported in Table X, with  $C_{1,k}$  acting as a “clock”. The weighted-voting parameter  $\nu$  defines instead the kind of resulting sequence: balanced Tausworthe 4B (T4B), when  $\nu = 4$ , or 2B (T2B), when  $\nu = 2$ . The ranging chip sequence can be easily generated by means of a sequential machine like the one depicted in Figure 26, composed of six shift registers, one per component, and a combinational circuit that performs that weighted voting.

Once again, the ranging signal expression appears quite cumbersome. However, if we assume for a moment that  $c_k \approx C_{1,k}$ , we obtain that  $\Phi(t) \approx \sin(\pi t/T_c)$ . Thus, by using again the Jacobi-Anger identity, we can approximate the PN ranging signal as

$$r(t) \approx J_0(m_r) + 2jJ_1(m_r)\sin(\pi t/T_c),$$

that is none other than a residual carrier with a frequency tone in  $1/2T_c$ . In reality, because of the other components,  $\{c_k\}$  deviates from the perfect clock, and other harmonics appear in the ranging signal. It can be shown that the first-order approximation reads [41]

$$r(t) \approx J_0(m_r) + 2j\xi J_1(m_r)\sin(\pi t/T_c),$$

where  $\xi$  is a coefficient that takes values in  $[0, 1]$ : the closer is to 1, the more  $\{c_k\}$  tends to be the ideal clock  $C_{1,k}$ . On the other hand, it can be shown that the acquisition time will be longer [41].

The two sequences T4B and T2B, have  $\xi = 0.9387$  and  $0.6274$ , respectively. If we think the clock  $C_{1,k}$  as the fundamental frequency tone, we realize that the T4B trades high position accuracy at the expense of a longer acquisition time. The other way round, the T2B allows to acquire the ranging sequence in shorter time but it will provide a poorer accuracy. Instead, for both PN sequences, the phase ambiguity is resolved by means of the other components  $C_{2,k}, \dots, C_{6,k}$  that, having a longer period, can be thought as the lower frequency tones.

As example, Figure 27 and 28 show the normalized PSD for the T4B and T2B signals, respectively, for  $m_r = 0.75$  rad/peak, with normalized resolution bandwidth  $R_{BW}T_c = 0.03$ . As expected, both spectra are characterized by a residual carrier component that has PSD equal to  $J_0(m_r)^2/R_{BW}T_c$  in correspondence of the carrier frequency, and PN components located at odd multiples of the clock frequency  $1/2T_c$ . Additionally, we can see the difference in power between the T4B and T2B clocks (i.e., the ratio of the two  $\xi^2$ ) being about 3.5 dB.

The range measurement, independently if done with code or PN ranging, needs to be complemented with range rate measurements. For this, the ground station estimates the range rate by measuring the Doppler on the TM signal. However, to avoid the spacecraft transponder frequency stability affecting the estimation, typically, the measurement is done in *coherent mode*. Namely, at TC arrivals, the transponder locks on the uplink carrier frequency and performs a turn-around, i.e., generates a TM signal whose carrier frequency is coherent with the uplink one, by means of a multiplicative ratio. The possible values of turn-around ratios depend on

the adopted frequency allocations and can be found in the ECSS [11]. For instance, if we consider a space mission having uplink and downlink in S-Band, with uplink frequency (say) 2030 MHz, ECSS foresees a turn-around ratio equal to 221/240. Consequently, the downlink frequency shall be  $2030 \cdot 240/221 = 2204.52$  MHz. Further details about the turn-around function will be given in Section IV.

#### E. Simultaneous communications and tracking

It is standard practice to simultaneously transmit information (telemetry/telecommand) while tracking the satellite. Generally, this is achieved through the combination (in phase) of a phase-modulated ranging signal  $r(t)$  and a residual carrier telemetry/telecommand signal  $s(t)$ . Mathematically,

$$s(t)r(t) = e^{jm_x x(t)} e^{jm_r \Phi(t)},$$

where the two exponential functions are the telemetry signal and the ranging signal as defined in (6) and (16), respectively. In the case of an NRZ/BPSK/PM telemetry signal and the code ranging, using the Jacobi-Anger identity and keeping only the first-order terms, we can see the overall signal approximated as

$$s(t)r(t) \approx J_0(m_x)J_0(m_r) + 2jJ_0(m_r)J_1(m_x)x(t) + 2jJ_0(m_x)J_1(m_r)\Phi(t), \quad (19)$$

where we can notice that the overall residual carrier is  $J_0(m_x)J_0(m_r)$ , while on the quadrature component we can find both the telemetry data and the ranging signal. For limiting the mutual interference between the information  $x(t)$  and the ranging tones of  $\Phi(t)$ , typically, the sub-carrier frequency  $f_x$  and the fundamental tone  $f_T$  are chosen “far enough” and exploiting the spectral nulls. More details about the selection of these two values can be found in [39].

A similar result can be obtained for a SP-L/PM telemetry signal by substituting in (19) the  $J_0(m_x)$  term with  $\cos(m_x)$  and  $J_1(m_x)$  with  $\sin(m_x)$ . Additionally, both the NRZ/BPSK/PM and SP-L/PM can be combined, as alternative, to a PN ranging signal by properly choosing the PN clock frequency [41].

If, on the one hand, low-rate residual-carrier modulated transmissions are either combined with the code or PN ranging, the standards establish high-rate suppressed-carrier signals (e.g.,  $> 1$  Msps) to be coupled with PN ranging only by using a GMSK-modulated telemetry signal [42]. Also, in this scenario, the telemetry signal acts as additional noise to the ranging. Vice versa, the latter disrupts the correct reception of the telemetry stream. For this reason, a proper choice of the two modulation indexes ( $m_x$  and  $m_r$ ) is required for managing the power sharing and the reciprocal interference, and it is strongly recommended to adopt interference cancellation schemes at the receiver (e.g., those provided in [42]).

#### F. Sizing of the links

In the previous sections, we provided a thorough description of the signals adopted for TC, TM, and RNG. In this section, we focus instead on their sizing for spacecraft missions by

Table X  
COMPONENTS OF THE PSEUDO-NOISE RANGING SEQUENCE.

Component	Period	Component period chips
$C_{1,k}$	2	+1 -1
$C_{2,k}$	7	+1 +1 +1 -1 -1 +1 -1
$C_{3,k}$	11	+1 +1 +1 -1 -1 -1 +1 -1 +1 +1 -1
$C_{4,k}$	15	+1 +1 +1 +1 -1 -1 -1 +1 -1 -1 +1 +1 -1 +1 -1
$C_{5,k}$	19	+1 +1 +1 +1 -1 +1 -1 +1 -1 -1 -1 +1 +1 -1 +1 +1 -1 -1
$C_{6,k}$	23	+1 +1 +1 +1 +1 -1 +1 -1 +1 +1 -1 -1 +1 +1 -1 -1 +1 -1 +1 -1 -1 -1

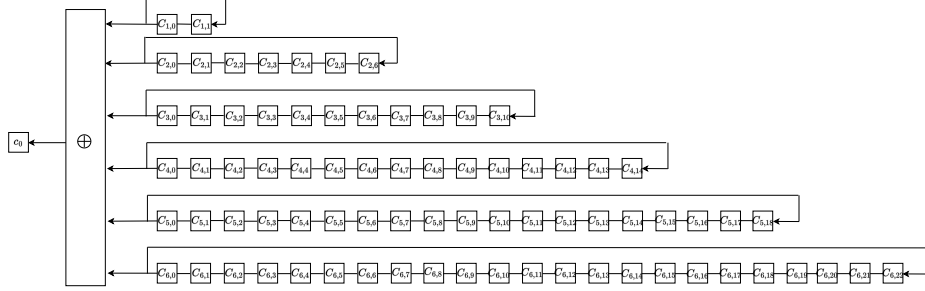


Figure 26. Sequential machine, loaded with the initial status, for generating the PN ranging sequence.

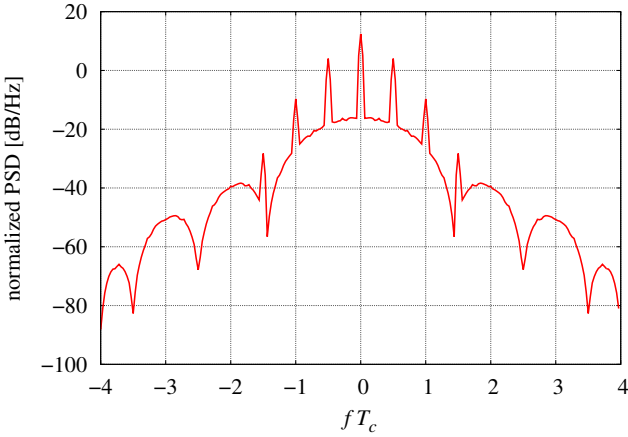


Figure 27. Normalized PSD for T4B PN ranging signal, modulation index  $m_r = 0.75$  rad/peak.

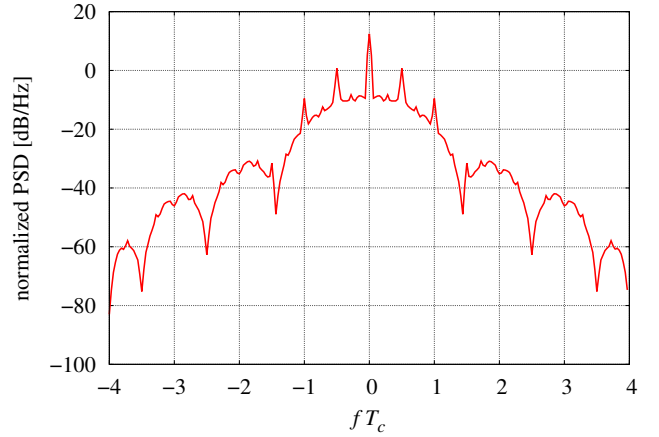


Figure 28. Normalized PSD for T2B PN ranging signal, modulation index  $m_r = 0.75$  rad/peak.

using a well known tool in telecommunications engineering: the link budget. The link budget determines the received power by summing up each loss and gain to which the transmitted signal is subject when traveling over the communication channel. The key formula that summarizes the link budget for a spacecraft mission is an instance of *Frijs transmission equation* [43] that in dB reads

$$\left(\frac{P_{RX}}{N_0}\right) = \text{EIRP} + \left(\frac{G}{T}\right) - L - k_B - \alpha, \quad (20)$$

where,  $P_{RX}/N_0$  is the ratio between received power and noise spectral density, EIRP is the effective isotropic radiated power,  $L$  the path loss,  $k_B$  is the Boltzmann's constant,  $G/T$  is the receiver gain over noise temperature of the receiver antenna, and  $\alpha$  includes other impairments/losses that the signal experiences before demodulation (atmospheric, pointing, demodulation,

etc.). Although the formula is rather simple, new engineers in the TT&C field can sometimes have difficulties in finding the right values to use and how to lay down a link budget in compliance with the standards. In this respect, this section focuses on the basics specific to the TT&C field.

For instance, the path loss accounts for the attenuation that the electromagnetic signal suffers during propagation from the transmitter to the receiver. Since satellite links crosses the free space, the path loss is defined, in logarithmic form, as

$$L = 20\log_{10}\left(\frac{4\pi sf}{c}\right),$$

where,  $f$  is the carrier frequency of the signal,  $s$  the distance, and  $c$  the speed of light. The distance  $s$  shall be the satellite *slant range*, i.e., the actual distance from the ground station (a function of the altitude and elevation angle).

The atmospheric loss, another relevant element in the link budget, is a highly variable parameter, strongly dependent on the weather and climatic conditions, hard to predict, and its estimation requires good knowledge of ITU-R models. Luckily, there are free available software tools that can help the TT&C engineer. For instance, CNES developed a dynamic link library to compute the atmospheric losses affecting the Earth-to-space and space-to-Earth transmission links [44].

Similarly, ESA makes available the tracking stations (ES-TRACK) facilities manual [13] that reports the characteristics of the ESA ground stations such as the  $G/T$ , ground station coordinates (needed for deriving the atmospheric losses), the adopted station modems (including possibly the demodulation losses), etc.

Traditionally, the link budget for spacecraft missions was computed for the worst-case scenario. However, the reader can easily realize that this method is inefficient: it contemplates the unlikely event in which all the terms involved in the computation simultaneously assume their worst-case value. To optimize the link budget and thus efficiently design the communication system, space missions usually adopt the procedures in the ECSS standard in [11]. According to this, one shall consider as many sets of parameters as the possible scenarios that involve different spacecraft antennas, ground stations, bit rate, etc., and compute a dedicated link budget for each. Focusing on one set, each of those parameters is characterized by its nominal, adverse and favorable values. We can identify the nominal and statistical approaches to compute the link budget. The former obtains the design SNR by summing up all the involved parameters assuming their nominal values. Alternatively, the second approach relies upon a statistical method [45] and is the best way to optimize the communication system design. It treats each parameter involved in the computation as a random variable characterized by a probability density function (pdf). Then, using the central limit theorem, the SNR is approximated by a Gaussian pdf. The ECSS standard [11] encloses a table listing all the probability distributions associated with the link budget parameters. Finally, to account for the uncertainties, both approaches add a margin.


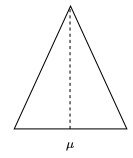
From practical experience, a margin of 3 dB is enough for the nominal link budget. For the statistical approach, [11] defines that the margin based on the *mean*  $-3\sigma$ , and *worst case root-sum-square* (worst case RSS) shall be higher than 0 dB.

In the following, we present a simplified example of a link budget computation for a TM link. We consider an hypothetical scenario of a TT&C transmission from an EO satellite, orbiting around 700 km above the Earth, with a minimum ground station elevation angle of 5 deg, to the Kiruna ground station, having  $G/T = 21.4$  dB/K. By using geometrical calculations, it is easy to see that the corresponding slant range  $s$  is 2563.13 km. For the TT&C we assume instead an S-Band subsystem,  $f = 2050$  MHz, as the one in Figure 2, having (nominal) RF output power  $-5$  dBW, antenna gain  $-3$  dB, and RFDN loss 4 dB. For the modulation and coding we consider a format that requires  $E_b/N_0 = 6$  dB and has bit rate  $R_b = 1024$  kbps.

Table XI  
EXAMPLE OF LINK BUDGET WITH NOMINAL, FAVORABLE, AND ADVERSE VALUES.

Parameter	Nominal	Favorable	Adverse
Altitude [km]	700	700	700
Elevation angle [deg]	5	5	5
Slant range $s$ [km]	2563.13	2563.13	2563.13
Frequency $f$ [MHz]	2250	2250	2250
RF output [dBW]	-5	-4	-6
Antenna gain [dBi]	-3	-2.9	-3.1
RFDN loss [dB]	4	3.9	4.1
EIRP [dBW]	-12	-10.8	-13.2
Path loss $L$ [dB]	167.7	167.7	167.7
Atmospheric loss [dB]	0.9	0.9	0.9
$G/T$ [dB/K]	21.4	21.5	21.2

Table XII  
PROBABILITY DISTRIBUTIONS AND STATISTICAL VALUES.

pdf	$\mu$	$\sigma^2$	$\Delta A^2$
 $G/T$ RFDN loss $\mu$	21.35 4	0.0075 0.0033	0.04 0.01
 Antenna gain RF output $\mu$	-3 -5	0.0017 0.1667	0.01 1

Given this input, we can derive that the EIRP is  $-12$  dBW and that the path loss is  $L = 167.7$  dB. Additionally, by using a software tool, we can find that the atmospheric loss at Kiruna, for a 99.9% availability and elevation angle 5 deg, is about 0.9 dB. We put all these values in a tabular form, as in Table XI and in line with the standards, for RF output, antenna gain, RFDN loss, and  $G/T$  we also define a favorable and adverse value<sup>7</sup>, and associate a pdf as reported in Table XII. We can then compute the mean  $\mu$ , the variance  $\sigma^2$ , and the adverse variation  $\Delta A^2$  (i.e., the square of the difference between the nominal and adverse value), and create a new link budget table as in Table XIII.

Now, we include in Table XIV the estimated SNR, obtained through the link budget calculation based on design values, mean  $-3\sigma$ , and worst case RSS. Namely, for computing the SNR for the design values, we apply (20) directly to the column ‘Nominal’ of Table XI, obtaining  $P_{RX}/N_0 = 69.44$  dBHz. For the mean  $-3\sigma$ , we repeat the same process on the column ‘ $\mu$ ’ of Table XIII, and decrease it by 3 times its standard deviation, i.e.,  $69.39 - 3\sqrt{0.1792} = 68.12$  dBHz. Finally, for the worst case RSS, we take the nominal value  $P_{RX}/N_0$  and decrease it by  $\sqrt{\Delta A^2}$ , i.e.,  $69.44 - \sqrt{1.06} = 68.41$  dBHz. As a final step, we can compute the residual

<sup>7</sup>It is pointed out that, without loss of generality, in this paper the favorable and adverse values are defined as absolute values. Differently in [11], these values are defined as variations w.r.t. the nominal values.

Table XIII  
EXAMPLE OF STATISTICAL LINK BUDGET WITH THE AVERAGE  $\mu$ ,  
VARIANCE  $\sigma^2$ , AND ADVERSE VARIATION  $\Delta A^2$ .

Parameter	$\mu$	$\sigma^2$	$\Delta A^2$
Altitude [km]	700	0	0
Elevation angle [deg]	5	0	0
Slant range $s$ [km]	2563.13	0	0
Frequency $f$ [MHz]	2250	0	0
RF output [dBW]	-5	0.1667	1
Antenna gain [dBi]	-3	0.0017	0.01
RFDN loss [dB]	4	0.0033	0.01
EIRP [dBW]	-12	0.1717	1.02
Path loss $L$ [dB]	167.7	0	0
Atmospheric loss [dB]	0.9	0	0
$G/T$ [dB/K]	21.35	0.0075	0.04
$P_{RX}/N_0$ [dBHz]	69.39	0.1792	1.06

Table XIV  
SNR COMPUTATION VIA THE THREE DIFFERENT LINK BUDGET  
APPROACHES.

Method	$P_{RX}/N_0$ [dBHz]	Margin [dB]	Required Margin
Design	69.44	3.34	$\geq 3$
Mean $-3\sigma$	68.12	2.02	$\geq 0$
Worst case RSS	68.41	2.31	$\geq 0$

margin for the three methods. The minimum SNR required is given by

$$\left(\frac{P}{N_0}\right)_{\text{req.}} = \frac{E_b}{N_0} + 10 \log_{10}(R_b),$$

that in our example is 66.1 dBHz. Thus we obtain that the three methods give a margin of of 3.34, 2.02, and 2.31 dB, respectively, in line with the ECSS requirement.

For improving margins, it might seem possible to increase the received SNR by enhancing the transmitted power, but this is not always a viable solution. In fact, to limit the risk of interference between communication systems, the ITU regulates the maximum *power flux density* (PFD), whose limits can be found in [11].

The PFD is a measure of the signal strength in the far field, and, assuming free space conditions, it is defined as

$$\text{PFD} = \frac{\text{EIRP}}{4\pi h^2} \max_{\mathcal{F}} \int_{\mathcal{F} - \frac{B_{ref}}{2}}^{\mathcal{F} + \frac{B_{ref}}{2}} S_s(f) df, \quad (21)$$

where  $S_s(f)$  is the normalized power spectral density of a generic transmitted signal  $s(t)$ ,  $h$  is the satellite altitude from the ground, and  $B_{ref}$  the reference bandwidth over which the PFD regulations apply. For suppressed carrier modulations, when the channel symbol rate  $R_s \gg B_{ref}$ , (21) reduces to

$$\text{PFD} \approx \frac{\text{EIRP} B_{ref}}{4\pi h^2 R_s}.$$

When residual carrier modulations are adopted, since the majority of the power is devoted to the carrier, (21) becomes

$$\text{PFD} \approx \frac{\text{EIRP}}{4\pi h^2} \alpha_c,$$

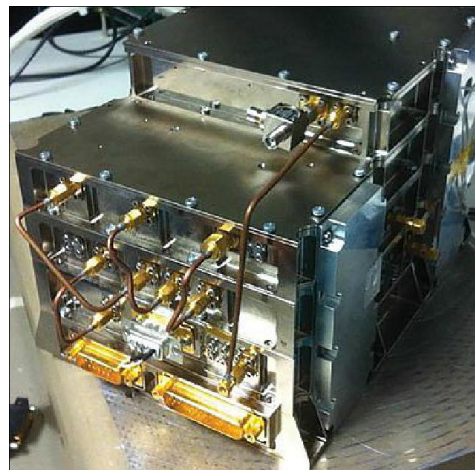


Figure 29. Engineering model of the ESA Solar Orbiter transponder. Image credit [7].

where  $\alpha_c$  is the carrier suppression, that is  $\cos(m_x)^2$  and  $J_0(m_x)^2$  for SP-L/PM and NRZ/BPSK/PM signals, respectively.

Notice that the EIRP to be adopted in the PFD shall be the highest value that can be experienced during the spacecraft mission. Additionally, the PFD for the residual carrier modulations is often the most critical and can dictate the maximum transmitted power. This particularly holds for TT&C systems that use a single RF power for multiple modulation and coding formats.

#### IV. THE TRANSPONDER

Having discussed the format of TT&C links, we have now the background knowledge for understanding the basics of a transponder architectural design, the main focus of this section.

As mentioned in Section II, the transponder is the core unit of the TT&C subsystem. It performs the TM transmitting and TC receiving functions while performing the RNG turn-around. To give the reader an idea of such a unit, Figure 29 shows the engineering model of the ESA Solar Orbiter mission [7]. The transponder is usually in the shape of a small box of about 20-25 cm per side, and organized into modules (e.g., one per layer, as shown in the figure) interconnected by means of external coaxial cables. Then, it can have different connectors/interfaces for the RF transmitter output, receiver input, power supply, and monitoring and control.

Although the transponder (as in the picture) is a quite complex unit, typically, its high-level architecture can be summarized as provided in Figure 30. It is composed by three modules: the RF down and up-conversion modules (to/from intermediate frequency, IF, for receiving and transmitting, respectively), and the digital module. These interface each-other using analog-to-digital and digital-to-analog converters (ADC, DAC). In turn, the transponder digital module interfaces with the spacecraft data-handling subsystem by means of dedicated electrical lines. For TC, the transponder provides the data-handling with the demodulated (but usually not decoded) TC data and the TC clock. This information is complemented with

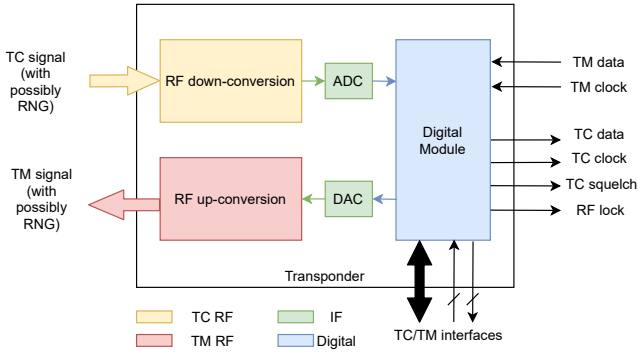


Figure 30. High-level architecture of a transponder unit.

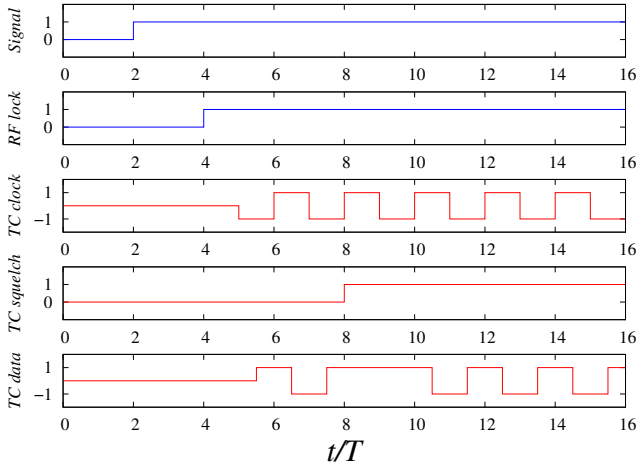


Figure 31. Sketch of the timing diagrams of the transponder TC interface to the data-handling subsystem.

a squelch signal (indicating the presence or not of valid TC data) and an RF lock status (specifying if the synchronization chain is locked on the received TC signal). Conversely, for TM, the data-handling provides the stream to be modulated by means of dedicated TM data and clock line.

To better understand the functional behavior of the data-handling lines, we reported in Figure 31 a sketch of the functional behavior of the TC interface. When the TC signal is received, the transponder receiver synchronization chain will take some time to close the loops. In the sketch (just for presentation purposes), this delay is reported as two symbol time  $T$ , after which the transponder declares the lock status on the RF lock electrical line. Then, after an additional delay, the transponder receiver will start to track the TC signal clock and demodulate the TC signal data, thus declaring the data validity through the TC squelch.

The monitoring and control function of the transponder is executed through a dedicated TC/TM interface (not to be confused with the two interfaces just described), in which the transponder receives internal TC from the data-handling for changing the configuration and provides the TM of its current status. The TC/TM interface is often implemented

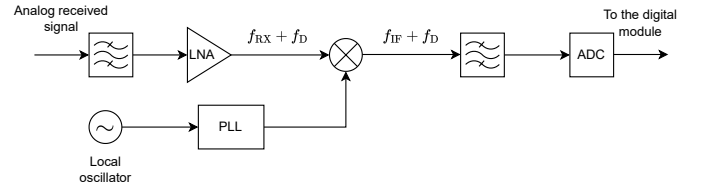


Figure 32. Basic block diagram of the RF down-conversion chain.

by means of a bi-directional bus and/or dedicated electrical lines. These last are usually preferable for essential TM (e.g., secondary voltage, temperature, etc.) and fundamental TC (usually known as *high priority command*, HPC), that could need to be collected or executed directly, bypassing the bus.

Although not visible in the high-level architecture of Figure 30, the transponder implements an RNG turn-around that (in naïve words) interconnects the receiver and the transmitting chains for having the so-called *RNG channel*<sup>8</sup>.

The following sections provide more detail about the functional behavior of the receiving and transmitting chains, in particular for the synchronization, demodulation, and RNG turn-around. For the sake of clarity, the description will be limited to the case of NRZ/PSK/PM signal for both TC and TM and the transparent turn-around of a code ranging signal. For the transmitter only, the case of filtered suppressed carrier modulation will be also provided. In all cases, it will be assumed that sampling rates are high enough for doing most of the signal processing into the digital core. However, these concepts can be easily extended to all other modulation formats and different digital/analog partitioning, and they are left to the reader for a more detailed study.

#### A. The receiving chain

The first stage the received signal goes through is the RF down-conversion module. This module can be rather complex, and include multiple stages of mixing, filtering, and amplifications. However, we can summarize its function with the basic block diagram shown in Figure 32. Here, after a first filtering process and a low-noise amplifier (LNA), the received signal frequency is down-converted from RF ( $f_{RX}$ ) to IF ( $f_{IF}$ ) through a local oscillator and a phase locked loop (PLL) serving as a multiplier. Once the signal is down-converted, the high-frequency components are cut out by a second filter before passing through the ADC. Then, the resultant digital signal reaches the digital module, whose demodulation function is strictly related to the modulation scheme adopted at the transmitting end.

In the case of NRZ/BPSK/PM, the digital module is composed of three main elements. First, a PLL for frequency/phase acquisition<sup>9</sup> and tracking, then a Costas loop which takes care of the sub-carrier tracking, and, finally, a data transition tracking loop (DTTL) for recovering the symbol timing.

<sup>8</sup>In case the unit does not have the RNG channel, then it is usually denoted as *transceiver* instead of transponder.

<sup>9</sup>It is pointed out that the carrier acquisition can be aided by the on-ground carrier sweeping procedure. According to this, the ground station transmits an unmodulated carrier that sweeps in a certain frequency range, for ensuring that enters in the PLL *lock-in range* [46].

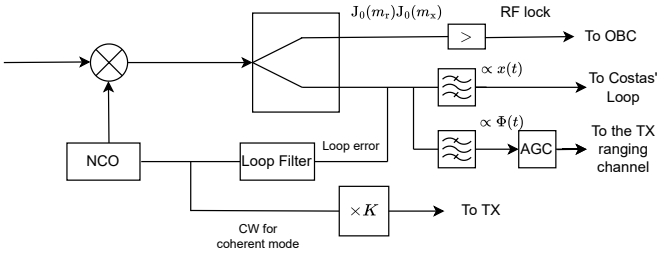


Figure 33. Block diagram of the receiver chain PLL, for the TC carrier frequency/phase tracking.

The block diagram of a PLL is sketched in Figure 33, where the circuit separates the in-phase and quadrature components of the received signal (a phase combination of telemetry and ranging signals) in two different branches. In line with the concepts expressed in Section III-E, when in lock, the uppermost branch carries the in-phase component  $J_0(m_r)J_0(m_x)$ , while the lower carries the quadrature component, split in turn (through filtering) in the telemetry and ranging component  $2J_0(m_r)J_1(m_x)x(t)$  and  $2J_0(m_r)J_1(m_r)\Phi(t)$ , respectively. The quadrature branch also acts as a loop error reference for computing the control word (CW) that controls a numerically controlled oscillator (NCO) that generates the local carrier. When the error is 0, i.e., the PLL is locked, the in-phase branch reaches a high value that acts as an indicator for setting the RF lock status. Moreover, whether the transponder is working in a coherent mode, as soon as the error becomes 0, the estimated frequency, scaled by the turn-around ratio ( $K$  in the figure), can be adopted by the transmitter.

Recalling the definition of NRZ/BPSK/PM, the data modulates a sub-carrier, which requires a tracking algorithm. Due to the presence of data, this can be done by means of a *Costas loop* [47], whose block diagram is sketched in Figure 34. In naïve words, Costas loop uses as an error the quadrature component of the sub-carrier multiplied by the data on the in-phase component for adjusting the sign. Hence, if the input of the Costas loop in complex base-band is  $a_k e^{j\phi}$  (where  $a_k$  are binary symbols, and  $\phi$  the sub-carrier phase error) the loop uses as error reference  $a_k^2 \cos(\phi) \sin(\phi) \approx \phi$ , when  $\phi$  is small.

It follows a DTTL for timing synchronization and consequently symbol demodulation, as depicted in Figure 35. The first component is an interpolator that aligns the input stream according to the estimated timing. Its output enters a mid-phase integrator which performs integration between pairs of adjacent bits. For obtaining the loop error, the mid-phase integrator output is then multiplied by the bit-transition, obtained as a difference between the current and the previous bit that passed through the in-phase integrator (matched filter). Depending on the sign of the filtered loop error, the interpolator controller, driving the interpolator, will anticipate or delay the estimated symbol time. Finally, as soon as the loop error becomes 0, the data valid status enables the OBC, provided with the data clock, to perform decoding of the data stream coming out of the matched filter.

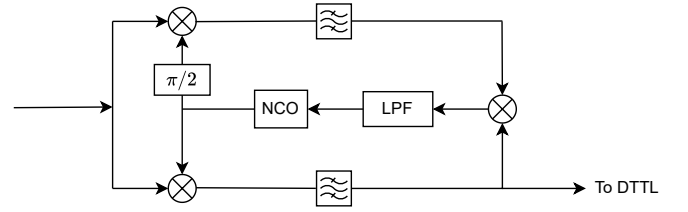


Figure 34. Block diagram of the receiver chain Costas Loop, for the TC sub-carrier tracking.

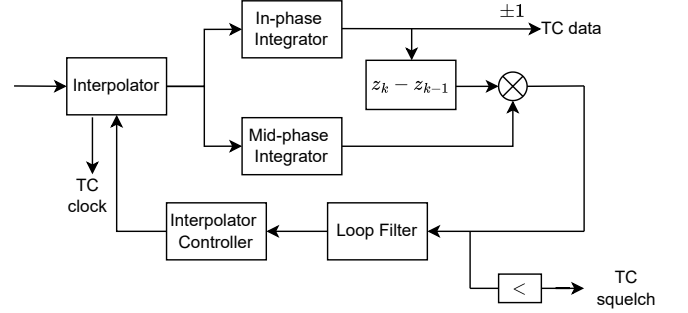


Figure 35. Block diagram of the receiver chain DTTL, for the TC timing synchronization.

## B. The transmitting chain

Figure 36 shows a possible digital implementation of the residual carrier transmitter with simultaneous transmission of the ranging signal. Starting from the right-hand side, a *coordinate rotation digital computer* (CORDIC, [48]) block generates the NRZ/BPSK signal as provided in (7). Namely, the TM clock, properly scaled, drives the clock of a phase accumulator, whose CW is chosen in a way for generating a sub-carrier phase  $\theta_i$  with samples

$$\theta_i = 2\pi f_x \left( \frac{i}{\eta} \right) T,$$

where  $\eta$  is the oversampling factor, and the sub-carrier  $f_x$  is a multiple of the TM symbol rate (see Table VI). The sub-carrier phase  $\theta_i$ , together with the (oversampled) TM data scaled by  $\pi/2$ , provides at CORDIC output the samples

$$\begin{aligned} x_i &= \cos \left( \theta_i - \frac{\pi}{2} a_{\lfloor i/\eta \rfloor} \right) \\ &= a_{\lfloor i/\eta \rfloor} \sin \left( 2\pi f_x \left( \frac{i}{\eta} \right) T \right), \end{aligned}$$

which correspond to the samples of  $x(t)$  in (7) at instants  $iT/\eta$ .

In turn, the NRZ/BPSK samples  $x_i$  are fed together with the ranging samples to a second CORDIC, with a carrier phase value that is controlled by a separated phase accumulator. The resulting signal has samples corresponding to  $s(iT/\eta)r(iT/\eta)$ , being  $s(t)$  and  $r(t)$  the target NRZ/BPSK/PM and ranging signals as in (6) and (16), respectively. Namely, the transmitted digital signal has complex base-band expression (w.r.t. the carrier frequency) equal to

$$s_i r_i = e^{jm_x x_i + m_r \Phi \left( \frac{i}{\eta} T \right)}.$$

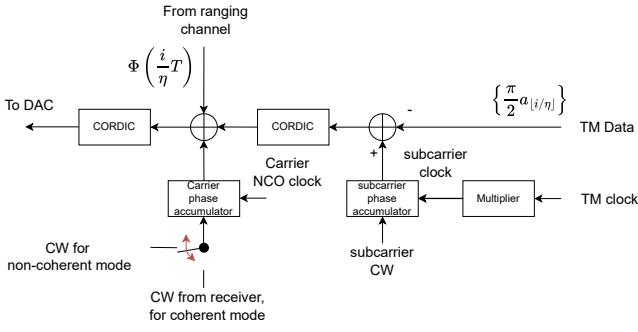


Figure 36. Block diagram for a possible implementation of a residual carrier TM transmitter, with ranging and coherency.

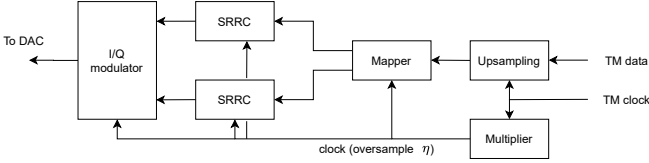


Figure 37. Block diagram of a possible implementation of a suppressed carrier TM transmitter for PSK/APS K signals.

The carrier phase accumulator can be properly tuned with a fixed CW for generating the target IF when in the non-coherent mode. Differently, for the coherent mode, the CW is provided by the receiver synchronization chain (see Figure 33). In this way, if the Doppler in uplink is equal to  $f_D$ , the transmitted signal becomes

$$s_i r_i e^{j2\pi K f_D (\frac{i}{\eta}T)}, \quad (22)$$

where  $K$  is the turn-around ratio.

The modulation of a suppressed carrier signal often requires a separated logic into the digital core, specially for those modulation formats that can be implemented by means of an I/Q modulator. Figure 37 shows a possible digital implementation of a PSK/APS K modulator. The TM binary symbol at its input are up-sampled by a factor  $\eta$  and mapped into PSK/APS K channel symbol, thus creating a stream whose I/Q parts (in complex-valued notation) read

$$\sum_k a_k \delta_{i-k\eta},$$

where  $a_k$  are channel symbols belonging to a PSK/APS K constellation, and  $\delta_i$  is the Kronecker delta. Such a stream is then SRRC filtered and I/Q modulated, thus producing a digital transmitted signal equal to

$$s_i = \sum_k a_k p_{i-k\eta}, \quad (23)$$

where  $p_i$  are the samples of the SRRC filter at instants  $iT/\eta$ .

For both the residual and suppressed carrier case, the digital transmitted signal in (22) and in (23) goes into a DAC. Its output is fed to the RF up-conversion chain that can be rather complex but with functions that can be summarized with the basic block diagram in Figure 38. The signal from the DAC is up-converted from IF ( $f_{IF}$ ) to RF ( $f_{TX}$ ), by means of a local

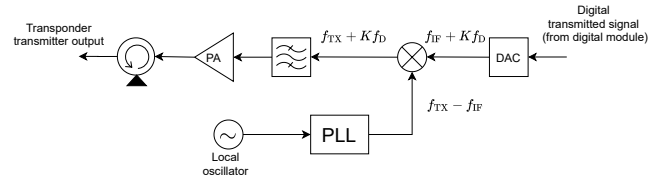


Figure 38. Basic block diagram of the transponder RF up-conversion chain.

oscillator and a PLL that provides the target frequencies. In the case of coherency, as shown in the block diagram, the up-conversion to RF is inclusive of the Doppler term  $Kf_D$ . Finally, the RF signal is fed to a filtering and power amplifier (PA) stage with the possible use of an isolator.

## V. LATEST TECHNIQUES AND THE (POSSIBLE) FUTURE OF TT&C

Now that we laid down the basics, this section tries to summarize some of the most relevant techniques and technologies that are coming up in the field, trying to give a picture of the (possible) future of the TT&C. In particular, the authors did their best to summarize the new techniques under consideration in future satellite missions. Nevertheless, this section is incomplete: even at the time of writing, many on-going studies could not be reported here for the lack of space and the sake of clarity. Thus, we recommend to the reader always check the latest available literature. A good reference is the proceeding of the triennial international workshop on TT&C [49].

### A. Variable coding and modulation

Most of the on-going and past satellite missions have a PDT subsystem that implements a single modulation and coding format (modcod) with a fixed bit rate. However, for low-Earth orbit (LEO) missions, such an approach has a major drawback: it does not take advantage of the SNR increase along the satellite pass.

To better understand this issue, let us assume a satellite with a PDT link having a fixed-rate QPSK of 1.0 Gbps, 1/2 coding rate (hence 1 GBaud), sized (link budget-wise) for a minimum ground station elevation that provides a pass of about 10 minutes. In Figure 39, the example is represented in cyan. Trivially, the total data volume will be 600 Gbit, i.e., 75 Gbyte. On the other hand, by doing some geometrical calculations, it is easy to show that the ratio between the maximum slant range  $s$ , and the minimum one (i.e., the satellite altitude  $h$ ) reads

$$\frac{s}{h} = \frac{1}{h} \sqrt{R_e^2 + (R_e + h)^2 - 2R_e(R_e + h)g(\phi_{\min})}, \quad (24)$$

where

$$g(\phi_{\min}) = \sin \left( \phi_{\min} + \sin^{-1} \left( \frac{R_e}{R_e + h} \cos(\phi_{\min}) \right) \right),$$

and  $R_e$  is the Earth radius. Considering the satellite in the example to have altitude  $h = 700$  km, and  $\phi_{\min} = 5$  deg, based on (24), we obtain a ratio of  $\sim 3.6$ , meaning that the

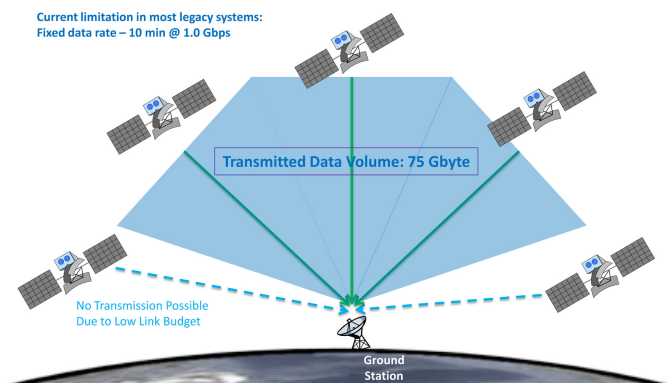


Figure 39. Example of satellite pass with a fixed-rate modcod. Image credit [50].

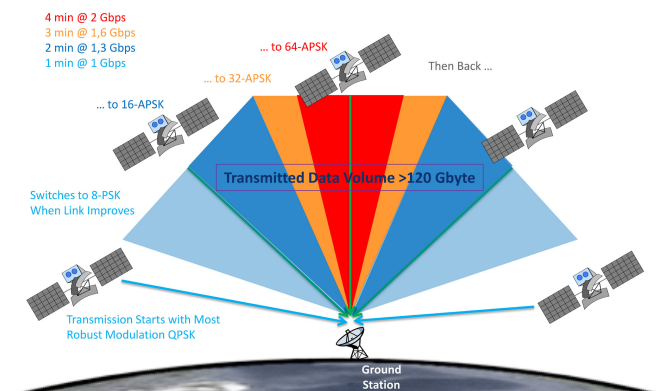


Figure 40. Example of satellite pass with different modcods implementing a VCM strategy. Image credit [50].

SNR will increase along the pass by more than 11 dB (see Section III-F).

Now, imagine taking advantage of this by increasing the bit rate by  $\sim 20\%$  every time that the SNR increases by 1 dB, up to 4 dB, and then, decrease the bit rate as the SNR decreases. The result will be a satellite pass like the one in Figure 40, where the satellite transmits (say) for 1 minute at 1 Gbps, 2 minutes at 1.3 Gbps, 3 minutes at 1.6 Gbps, and (at zenith) 4 minutes at 2 Gbps. This gives a data volume of about 123 Gbyte, with a 64% increase w.r.t. the fixed-rate modcod. This technique is known as *variable coding modulation (VCM)*, which consists of nothing else than defining a schedule of modcods along the satellite pass for changing the bit rate as the path loss changes.

Although the concept can appear quite basic, some technical aspects are not trivial and need to be mentioned. Namely, the change of bit rate shall not cause any link loss or additional overhead/inefficiency not to lose the advantage gained using VCM.

For doing this, we first need a suitable physical layer standard. In this respect, CCSDS defined the VCM standard in [51] for which ESA future missions plan to adopt the instance known as *type 1*, based on serially concatenated convolutional codes (SCCC). The full specification of type 1 - SCCC can be found in [52] (often known in the TT&C

Table XV  
CCSDS 131.2 ModCodS.

ACM	Modulation	bit/ch. symbol
1	QPSK	0.71
2	QPSK	0.86
3	QPSK	1.04
4	QPSK	1.21
5	QPSK	1.39
6	8PSK	1.63
7	8PSK	1.39
8	8PSK	1.63
9	8PSK	1.84
10	8PSK	2.10
11	8PSK	2.37
12	8PSK	2.64
13	16APSK	2.37
14	16APSK	2.64
15	16APSK	2.90
16	16APSK	3.20
17	16APSK	3.50
18	32APSK	3.20
19	32APSK	3.50
20	32APSK	3.82
21	32APSK	4.12
22	32APSK	4.44
23	64APSK	4.12
24	64APSK	4.44
25	64APSK	4.77
26	64APSK	5.06
27	64APSK	5.39

community, with abuse of naming, simply as *SCCC standard*). This standard foresees 27 modcods, as shown in Table XV, with five PSK/APSK modulations, different coding rates, and efficiency ranging from 0.71 to 5.39 bit per channel symbol. During transmission, the information symbols are organized into a physical layer frame, as shown in Figure 41. The frame starts with a marker of 256 fixed channel symbols for recognizing the beginning. The marker is followed by the frame descriptor, composed of 64 channel symbols encoding (with strong protection) 6 bits that identify the adopted modcod and the optional use of pilots. Both frame marker and descriptor are  $\pi/2$ -BPSK modulated. It follows the information block that includes 129 600 channel symbols with the selected modcod. Then, the information block can optionally contain blocks of 240 pilots,  $\pi/2$ -BPSK modulated, every 8100 channel symbols for improving synchronization. This special data structure allows the transmitter to change the modcod at each frame: the receiver simply has to maintain the synchronization based on the frame marker and pilot fields and identify the modcod adopted in each frame by decoding the descriptor. If we consider the example provided at the beginning of this section, the modcod can be changed every 0.13 milliseconds while having a total overhead of less than 4%.

As a second technical aspect, we need to properly select the operational point of the PA in the RF up-conversion chain (see Section IV-B). The operational point shall be selected as a trade-off between amplifier nonlinear distortions against transmitted RF power. Considering that, different coding rates allow coping with different levels of nonlinear distortions, each modcod has an optimal output back-off (OBO) [53]. Hence, to achieve the best performance, the VCM transmitter shall change the OBO at the beginning of each frame and needs to be implemented by having a proper loop between the RF

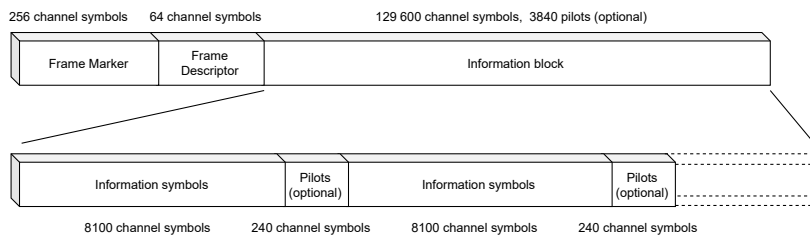


Figure 41. VCM type 1 - SCCC, physical layer frame structure. It is composed by a frame marker (for recognizing the start of frame), a frame descriptor (for identifying the adopted modcod), and an block containing the information channel symbols with (optionally) pilots for aiding the synchronization.

up-conversion chain and the digital board for adjusting the power level control. For more information about the OBO optimization for the SCCC standard, the reader can refer to [54].

As a final remark, although there are not yet (flying) ESA spacecraft implementing VCM, such a technique is considered a baseline in many EO future missions and has also been proposed recently for future SRS missions [55].

### B. Adaptive coding and modulation and re-transmission protocols

Although VCM is very promising, the data volume achieved can be further increased by taking advantage of the residual margin that raises by random effects, especially atmospheric losses. Namely, as described in Section III-F, the link budget usually allocates a dedicated margin for these effects, that in specific cases can result in a large inefficiency. This is particularly true for LEO missions (mostly EO) with a PDT at high frequency.

To give the reader a better idea, let's consider the EO mission described in Section III-F. We have seen that the atmospheric loss in S-Band, for an almost complete annual availability (99.9%) at Kiruna, with 5 degree elevation, are very low and not an issue. However, if we recompute the atmospheric loss assuming a K-Band link, this would result in about 24 dB, mostly due to the rain attenuation. Differently, for 95% availability, we get 7 dB. This means that we waste  $24 - 7 = 17$  dB in the link budget just for avoiding long outages in about 20 "bad days" per year. For the remaining days, the spacecraft link will experience instead a squandered high SNR (especially during sunny days).

Imagine now erasing (part of) this margin, and having a ground station that is able to perform an (almost) real-time SNR estimation for deriving the "link quality". During the pass, the ground station can then send TCs on how to switch the bit rate instantaneously based on the link quality, thus using an *adaptive coding modulation* (ACM) approach, that takes advantage always of the best conditions while implementing also VCM.

From a spacecraft communication subsystem architecture, the use of ACM appears almost as transparent. It is sufficient that the PDT subsystem implements a VCM standard (as provided in the previous section) and it can change the modcod as soon as the related TC is received.

Differently, on the ground segment, things are more complex. Regarding Figure 1, the ACM strategy shall be imple-

mented on the payload TM link: the payload ground station has to measure the link quality, reports it to the MOC that, in turn, will select the modcod, and send the TC to the spacecraft by means of the TT&C ground station. Thus, there are the following major challenges:

- payload ground station and MOC needs to close the loop by means of protocols that today are not well defined;
- the overall delay from link quality measurement till change of the ACM should be as short as possible, at least faster than atmospheric losses coherence time (with respect to the overall spacecraft channel dynamic);
- in turn, the TT&C ground station and payload ground station should be as co-located as possible in order not to limit the satellite pass interval in which ACM can be implemented.

At the time of writing, ESA already conducted dedicated studies on ACM (e.g., [56], [57]), and it is internally performing research activities for considering ACM for (possible) implementation in future EO missions.

As an alternative and intermediate step, ESA is currently considering instead to adopt a re-transmission protocol known as *CFDP Class 2* that can be seen somehow as ACM implemented at protocol level since it causes a reduction of the net bit rate. Namely, future EO missions using K-Band (like ROSE-L [58]) will have a link budget sizing between 95-99% availability. Instead, the link outages occurred during rainy days will be recovered through data re-transmissions. For further information about CFDP Class 2 functions and performance, the reader can refer to [59]–[61].

### C. Simultaneous transmission of high-rate telemetry and PN ranging

As mentioned in Section III-E, for transmitting high-rate telemetry with ranging, standards foresee the simultaneous transmission of PN ranging with high rate GMSK-modulated telemetry [42]. This scheme is highly adopted in SRS missions transmitting in X-Band. On the other hand, for increasing the spectral efficiency, SRS missions (especially near Earth) are considering the adoption of high-order modulations (like those in the SCCC standard [52]) for potentially enabling also the use of VCM [55].

For this reason, the authors in [62] performed a feasibility study on the coupling of PN ranging with high-order

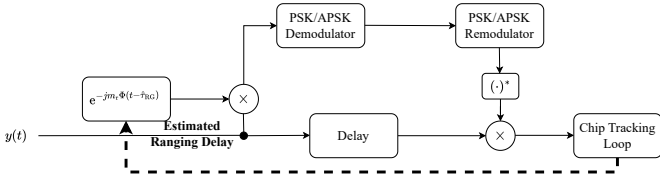


Figure 42. Block diagram of a receiver that allows the simultaneous demodulation of a PSK/APSK modulated signal and tracking of the PN ranging.

PSK/APSK modulations. Namely, it was considered a SRRC-filtered PSK/APSK-modulated telemetry stream reading

$$s(t) = \sum_k a_k p(t - kT),$$

where  $T$  is the channel symbol time,  $p(t)$  is the SRRC pulse shape, and  $\{a_k\}$  are channel symbols belonging to a PSK/APSK modulation. At the transmitter, the telemetry stream and the phase-modulated ranging signals are multiplied (in complex base-band) as

$$s(t)e^{jm_r\Phi(t-\tau_{RG})}$$

where  $\Phi(t)$  is the PN ranging of (18), and  $\tau_{RG}$  a generic delay between the two signals.

In the study, it was investigated a receiver scheme that can simultaneously demodulate the telemetry data while tracking the ranging signal. Figure V-C shows the receiver block diagram, where there are two parallel branches in a closed loop: one responsible for demodulating the telemetry signal, while the other for tracking. Namely, the upper branch first cancels out the ranging from the received signal by using a locally generated replica and performs demodulation and regeneration of the telemetry signal. Then, the parallel branch performs a complex multiplication for canceling the telemetry signal, and obtaining the ranging signal that goes in input to the chip tracking loop. The latter tracks the ranging sequence and feeds back the estimated time delay  $\hat{\tau}_{RG}$  to the local PN ranging generator.

For this scheme, it was found that the timing jitter has a closed form approximation reading

$$\sigma_\tau^2 \approx T_c^2 \left( \frac{1}{8} \frac{N_0 B_L}{P} + \frac{\sigma_\zeta^2 B_L T_c}{2} \right), \quad (25)$$

where  $T_c$  is the chip time,  $B_L$  the chip tracking loop bandwidth,  $P$  the useful power of the ranging signal, and  $\sigma_\zeta^2$  the normalized sum of the coefficients of the correlation between the ranging and the telemetry signals. It is interesting to notice that, while the first term encloses the classical dependency from the SNR in the loop, the second term underlies a floor caused by an additional noise due to the telemetry signal. Namely, it can be shown that this noise term is due to the non-constant envelope property of the telemetry stream that, differently from GMSK, cannot be perfectly canceled out from the ranging signal.

The performance results presented in [62] indicate the feasibility of adopting such a communication scheme. In fact, besides the ranging and telemetry reciprocal interference, the

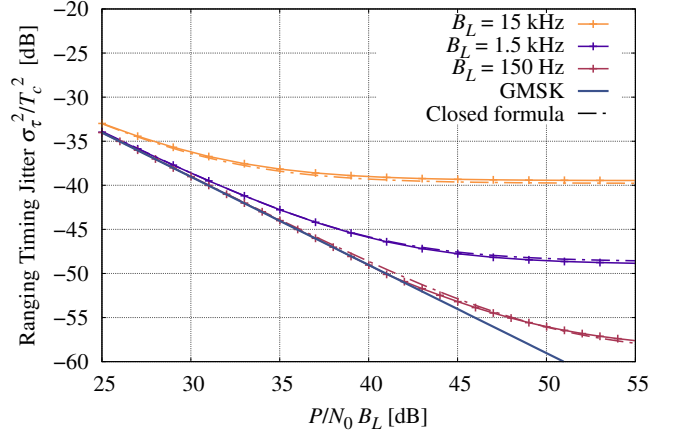


Figure 43. Ranging timing jitter for QPSK, SRRC having roll off 0.2, with PN ranging,  $m_r = 0.45$  rad/peak, for different values of the loop bandwidth  $B_L$ .

BER does not suffer significant degradation, while the ranging timing jitter reveals a floor that, as highlighted by (25), can be decreased by lowering  $B_L$ . This behavior is evidenced by Figure 43, which shows the timing jitter, normalized to  $T_c^2$ , obtained with a receiver that perfectly demodulates the telemetry symbols. In the figure, the telemetry is a QPSK-modulated signal with a roll-off factor of 0.2, while the ranging modulation index is  $m_r = 0.45$  rad/peak. Despite the jitter floor, the tracking capabilities are comparable to the case of adopting the classical GMSK (depicted in blue) when lowering the loop bandwidth.

#### D. TC LDPC codes

The use of BCH(63,56) for TC links is very well suited for short and low-rate (i.e., few kbps) communications, especially for links that transmit the required commands a few times a day. However, the BCH has a limited coding gain and, considering the ever-increasing need of higher bit rates, it can sometimes become a major design driver. For instance, a spacecraft could require just for TC communications to embark an additional (and more directive) antenna in addition to the two classical LGAs (see Section II). For this reason, the CCSDS defined two LDPC codes that have higher coding gain than the one provided by the BCH code. Since 2021, these two codes are also part of ECSS [28].

The two LDPC codes, usually denoted as LDPC(128,64) and LDPC(512,256), are systematic with rate a 1/2 and encode 64 and 256 bits into 128 and 512 bits, respectively. For having a good balance between encoding/decoding complexity, coding gain, and coding rate, these codes were designed with a circular structure (more details can be found in [33]). Figure 44 shows the bit error rate (BER) for the two LDPC codes, for a BPSK signal, and as a function of the energy-per-bit over noise spectral density  $E_b/N_0$ . For comparison, the BER of the uncoded and BCH-coded (SEC and TED) BPSK are also included. It can be seen that LDPC can provide an additional coding gain of 3-5 dB w.r.t. BCH, thus making them particularly attractive for future missions.

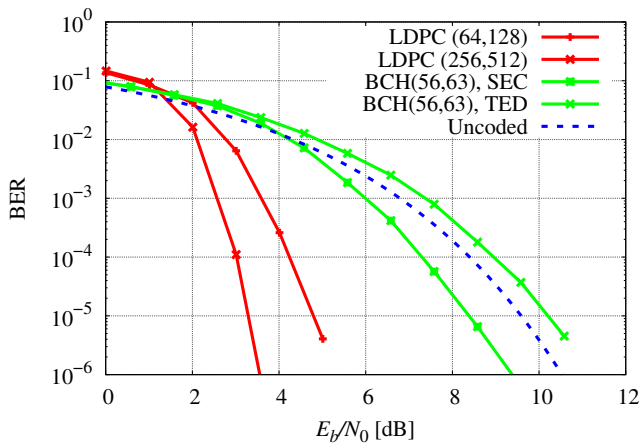


Figure 44. BER curves for a BPSK signal that is coded with LDPC(64,128), LDPC(256,512), BCH(56,63), or BPSK uncoded.

On the other hand, to make the LDPC compatible with the PLOP-2, the CLTU structure as described in Section III-B (and shown in Figure 15) shall be modified. In particular, the start sequence is modified with a 64-bit pattern, while the tail sequence is a 128-bit pattern that can be optionally used for LDPC(128,64), while it shall be never used for LDPC(512,256). This change takes into account the error correction and detection capability of the two LDPC codes. It allows the user to decide either to have the tail sequence for detecting the end of a CLTU (as for the BCH) or, to have the LDPC decoder to fail the decode when it over-runs the CLTU. For further information about the design choices for the two LDPCs and the summary of performance, the reader can refer to [33].

### E. Delta differential one-way ranging

As described in Section III-D, the TT&C subsystem has a tracking function that allows to obtain the range and range rate measurements. However, these two measurements are insufficient for the spacecraft orbit determination: the missing coordinates are estimated by means of the ground station motion as Earth rotates. The overall accuracy of this approach can be in the order of few meters and millimeters/seconds, that is usually more than sufficient for a large variety of missions. On the other hand, these figures could result quite poor for scientific missions that have to perform critical maneuvers (as gravity assist sling-shots and orbit insertions [1]) or radio-science measurements [63].

The *delta differential one-way ranging* (DDOR) is a technique that increases the accuracy of the tracking [64]. Basically, the DDOR measurement is carried out by transmitting a dedicated signal to two ground stations, and computing the differential delay. For a better understanding of the concept, let us assume a spacecraft that transmits a pure tone signal, with frequency  $f_T$ , that is received simultaneously by two ground stations as in Figure 45. If the spacecraft is in deep space, the signal path differential between the two ground stations will be approximately  $d_{GS} \cos(\phi)$ , being  $d_{GS}$  the distance between

Table XVI  
TONES NUMBER AND (APPROXIMATED) FREQUENCIES TO BE ADOPTED FOR DDOR.

Allocation	$I$	$f_{T,i}$
S-Band	1	$\sim 1$ MHz or $\sim 4$ MHz
X-Band (deep Space)	2	$\sim 1$ MHz or $\sim 4$ MHz, and $\sim 20$ MHz
Ka-Band	3	$\sim 1$ MHz or $\sim 4$ MHz, $\sim 20$ MHz, $\sim 76$ MHz

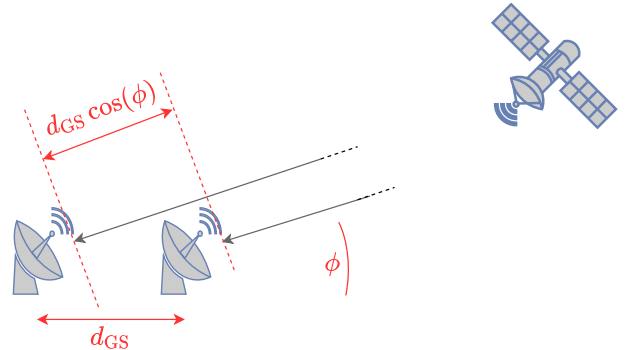


Figure 45. Sketch illustrating the basics of DDOR: the signal sent from the spacecraft is received simultaneously from two ground stations, for estimating the elevation  $\phi$ .

the stations, and  $\phi$  their elevation to the spacecraft. Now, if we measure the phase difference  $\Delta\theta$  of the signal as received by the two stations, we can estimate the elevation angle as

$$\hat{\phi} = \cos^{-1} \left( \frac{\Delta\theta}{2\pi f_T d_{GS}} \right), \quad (26)$$

thus obtaining an additional measurement for the orbit determination. In practice, the DDOR relies on a more complicated mathematical framework: Equation (26) shall be extended to three dimensions, and the DDOR signal comprises multiple tones. On the other hand, the underlying concept stays the same.

The DDOR waveform, as defined in the CCSDS standard [25] (recommendation 2.5.6B), is a phase modulation as in (16) where the phase  $\Phi(t)$  is

$$\Phi(t) = \sum_{i=1}^I \sin(2\pi f_{T,i} t), \quad (27)$$

being  $I$  the number of tones, and  $f_{T,i}$  the frequency of the  $i$ -th tone, to be chosen as provided in Table XVI depending on the carrier frequency allocation.

Although the concept appears quite simple, the DDOR measurement is a complex operation. Namely, the differential phase is affected by several factors: spacecraft thermal noise, ground station oscillator stability, atmosphere, solar plasma, etc. To mitigate the jitter caused by these factors, the ground stations adopt a quasar for performing a calibration, as sketched in Figure 46. Quasar catalogs are sufficiently dense with sources in S-, X-, and Ka-Band allocations for deep space links and with a position known in the order of nrad. Thus, the ground stations use as reference a quasar in the same frequency of the transmitted signal, and usually within 0.15 nrad from the spacecraft, so that quasar's and spacecraft's signal path and effects through Earth's atmosphere are similar.

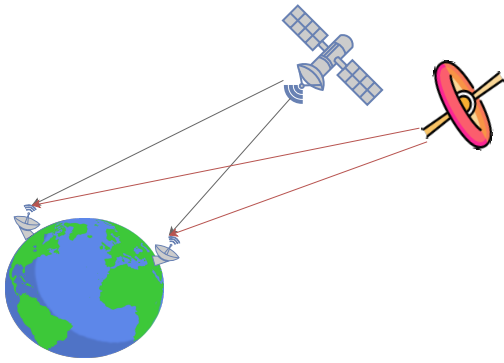


Figure 46. Sketch of the DDOR technique: a reference quasar (in red) is adopted for the calibration of the two ground stations. Subsequently, the two ground stations receive simultaneously the DDOR signal from the spacecraft for performing the measurement.

At time of writing, the DDOR has been adopted in major ESA deep space missions, like *Rosetta*, showing very good performance. However, CCSDS is currently working on an improved version: the *wide-band DDOR* (also known as PN DDOR, [65]). In particular, one of the major impairment in the DDOR measurement is the instrumental phase dispersion, caused by the spectral difference between the quasar (a broadband signal) and the spacecraft signal (composed by pure tones). For reducing the spectral difference, the spacecraft can thus modulate a wide-band DDOR signal, with a PN sequence on a sub-carrier as

$$\Phi(t) = \left( \sum_k c_k h(t - kT_c) \right) \sin(2\pi f_T t),$$

being  $c_k$  the sequence of chips,  $T_c$  the chip time, and  $h(t)$  a SRRC shaping pulse. While the standard that will provide chip definition, chip rate, and SRRC roll-off is still under definition, in general these shall be selected for matching as much as possible the quasar signal, while being feasible for hardware implementation. Usually, this is accomplished by resorting to small roll-off factors (e.g., 0.1) and chip rate in the order of several Mcps. For instance, Figure V-E shows an example of spectrum for a signal filtered with roll-off factor of 0.1, modulation index of 0.5 rad/peak, and a chip rate of about 7.2 Mcps. As it can be seen, the modulated sub-carrier provides a lobe rather flat, thus resembling the quasar.

#### F. Survey of additional techniques

Beyond the techniques here presented, there are several ongoing TT&C and PDT studies that we are unable to describe more in detail because of the lack of space. Hence, this section aims to provide a quick survey of some of these studies with related references the reader can peruse for his/her detailed studies.

As first, we mention the *telemetry ranging* technique. In naïve words, telemetry ranging is a modulation method that makes the ranging delay measurement completely digital. The spacecraft, instead of transmitting in downlink a replica of the received ranging signal (see Section III-D), samples its code phase and encodes it into 40 bits of the TM transfer frame.

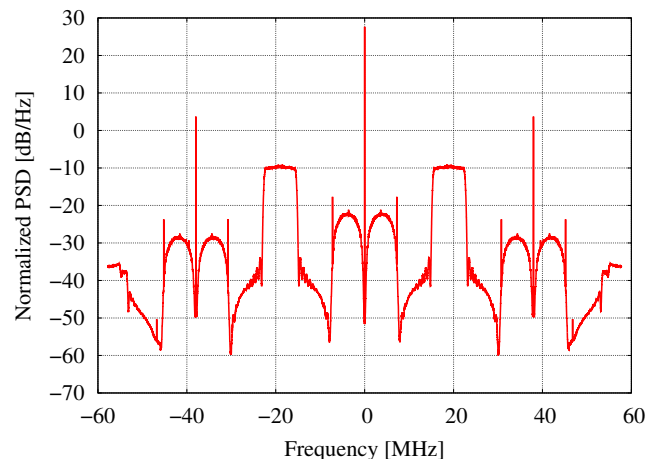


Figure 47. Wide-band DDOR spectrum with modulation index 0.5 rad/peak, roll-off factor 0.1, and chip rate 7.2 Mcps.

This technique has been initially proposed and implemented as a prototype by NASA in the studies [66]–[68]. Currently, ESA is performing internal studies on whether to consider it or not for implementation. Meanwhile, CCSDS has instead published a general recommendation (2.4.24 in [25]) that agencies can adopt as a reference.

As second novelty, we mention the *exploitation of the X-Band EESS allocation* for EO missions. As summarized in Table III, such missions usually have a TT&C subsystem in S-Band, and a dedicated X- or K-Band PDT subsystem. However, the ever-increasing number of satellites are making the S-Band congested, causing a complex frequency coordination between the different space agencies and administrations. In light of this, the ITU in 2015 agreed a new frequency allocation in X-Band uplink, in addition to the existing S-Band. This allows TT&C engineers to design an *integrated TT&C and high-rate PDT transponder*, that couples the functions of the two subsystems. Recently, ESA funded two studies for implementing a breadboard of such kind of transponder [69], [70].

On a similar topic, we report the *exploitation of the K-Band allocation* for high-rate links. As discussed so far, spacecraft usually have an uplink just meant for TC. However, with the increased interest in human and robotic exploration around the Moon, future space missions plan to have high-rate telemetry-like links also Earth-to-space (e.g., for connecting a human outpost to Earth). In this respect, entities such as CCSDS and SFCG are paving the way for standardizing such links in the K-Band allocation 22.55–23.15 GHz. Instead, space agencies are performing activities for developing high-rate K-Band spacecraft receivers and ground station transmitters, like the ESA ones in [71], [72].

As a final topic of particular interest, we report the *multiple spacecraft per antenna aperture* (MSPA) [73]. Currently, ground stations can only serve one spacecraft at a time. However, for planetary missions (like Martian ones), the ground station beamwidth is able to cover multiple orbiters and landed assets. Thus, instead of having dedicated one-to-one communications for each spacecraft, the ground station

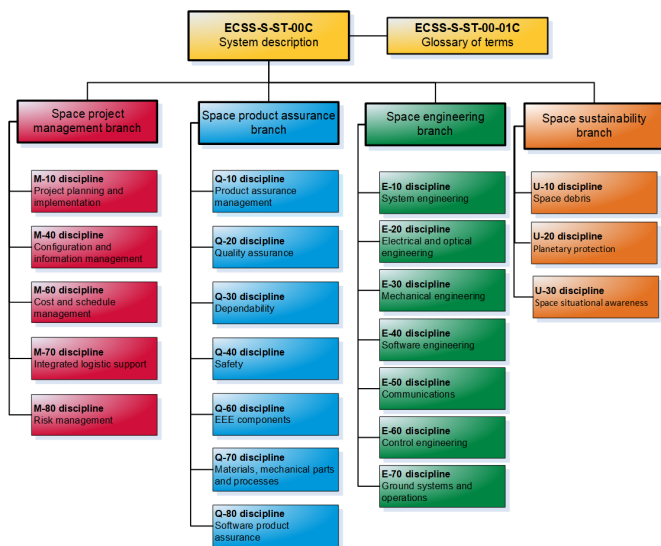


Figure 48. ECSS standards organizational structure, as per 15 September 2021. Image Credit www.ecss.nl.

could send TC and receive TM simultaneously from multiple spacecraft. For doing this, the use of a special code division multiplexing and multiple access scheme has been selected. This technology is currently under development in future transponders and ground stations transceivers [74], [75].

## VI. STANDARDIZATION

Throughout this paper, we often referred to applicable standards as ECSS, CCSDS, and SFCG. These standards are sometimes “intertwined”, creating a complex framework that even well-experienced TT&C engineers can sometimes have difficulties understanding it.

The objective of this section is to explain the basics of the organization of space communications standardization and provide the reader with a summary of the applicability of these standards for the design of TT&C subsystems. In particular, a short overview of ECSS and its standard organizational structure will be given in Section VI-A, while Section VI-B and VI-C will provide a brief description of CCSDS and SFCG, respectively, trying to highlight how their standards shall be adopted as a complement to the ECSS.

### A. ECSS

The European cooperation for space standardization (ECSS) is an initiative established to develop a coherent, single set of standards for use in all European space activities. ECSS includes as members major European agencies such as ESA, CNES, DLR, ASI, UKSA, etc., and a European industry representation.

Figure 48 shows the ECSS organizational structure of the active standards. They are organized into four main branches: space project management, product assurance, engineering, and sustainability, identified by the letter M, Q, E, and U, respectively. On top of these, there is the system (S) branch. In

turn, all the four branches are divided into disciplines identified with a serial number ranging from 10 to 80.

For TT&C, the main discipline is *E-50, communications*, and thus all relevant standards have an identification in the format *ECSS-E-x-50-n*, where *x* is the kind of document, and *n* is a number for identifying the standard, followed by a letter for indicating the revision. The E-50 includes (at the time of writing) 17 standards. Limiting to those dealing with the topics of this paper, we can limit the discussion to those shown in Table XVII. This list includes:

- a general standard *Communications* covering definitions, subsystem requirements, and activities to be performed for the design, implementation, and validation of space communication subsystems;
- *ranging and Doppler tracking*, providing full details about the code ranging described in Section III-D, and requirements to be respected for not impacting the tracking performance;
- the standards for TC and TM modulations and coding formats (as summarized in this paper in Section III-B and III-C, respectively), but including also frequency allocations (as reported in Section II-B), spectrum management and spectral requirements (for compliance to ITU/RR and meeting specific performance), and impairments limitations (e.g., maximum phase noise and minimum carrier suppression).

Most of the time, ECSS provides a sufficient set of requirements for the design of TT&C subsystems. It captures and properly traces the outcomes from the other standardization groups, or it makes even directly applicable their standards (e.g., see two CCSDS *Adoption Notice* shown in Table XVII). Hence, ECSS E-50 can be often adopted as a starting point. On the other hand, the TT&C engineer has to keep in mind that there are some exceptions: advanced TT&C techniques, novel formats, etc., are not always covered, and one has to refer directly to the other standardization groups. In addition, ECSS sometimes performs some tailoring of the applicable standards. Some of these exceptions are reported in the following sections.

### B. CCSDS

The consultative committee for space data systems (CCSDS) is an inter-agency standardization group that develops standards for data-systems and information-systems to promote interoperability and cross-support among cooperating space agencies. It is (at the time of writing) composed of 11 member agencies (including space agencies such as ESA, NASA, JAXA, and ROSCOMOS), 32 observer agencies, and over 119 industrial associates.

Standards are organized in *blue books*, and supported by informative reports, known as *green books* that contain descriptive material, analysis, test results, etc. On top of these, there are also experimental standards, denoted as *orange books*.

With reference to the content of this paper, the main blue books of reference are the *Radio Frequency and Modulation Systems* [25], *TC synchronization and channel coding* [31],

Table XVII  
SUMMARY OF THE RELEVANT ECSS E-50 STANDARDS THAT DEALS WITH THE TT&C TOPICS DISCUSSED IN THIS PAPER.

Identification	Title	Description
ECSS-E-ST-50, [34]	Communications	high-level standard that includes: <ul style="list-style-type: none"> <li>• definitions,</li> <li>• communication system requirements (e.g., redundancy, command priorities, etc.),</li> <li>• activities to be performed for the design, implementation, and validation.</li> </ul>
ECSS-E-ST-50-02C, [39]	Ranging and Doppler tracking	standard that defines the code ranging (see Section III-D) and requirements about transponder coherency, turn-around, group delay, etc., that directly impact the tracking performance.
ECSS-E-ST-50-05C, [11]	Radio frequency and modulation	standard that defines: <ul style="list-style-type: none"> <li>• the modulations for TC and TM (Sections III-A, III-B, III-C),</li> <li>• spectrum management and spectral requirements,</li> <li>• impairments limitation.</li> </ul>
ECSS-E-AS-50-21C, [38]	Adoption notice of CCSDS TM synchronization and channel coding	document that makes applicable the CCSDS standard for TM synchronization and channel coding (as described in Section III-C), but with specific tailoring for ECSS.
ECSS-E-ST-50-24C, [32]	Adoption notice of CCSDS TC synchronization and channel coding	document that makes applicable the CCSDS standard for TC synchronization and channel coding (as described in Section III-B), but with specific tailoring for ECSS.

and *TM synchronization and channel coding* [37]. The reading of these standards is well complemented by the following green books: *Bandwidth-Efficient Modulations* [26], which provides a review of filtered PSK and GMSK with details on their implementation, and *TC/TM synchronization and coding*, giving a summary of concept and rationale [33], [76].

Since many ECSS agencies are also CCSDS members, the standards for TT&C are usually well aligned with the corresponding ECSS ones. However, we report here some major differences:

- *TC modulation, coding, and synchronization*: according to CCSDS, the BPSK modulation can be also considered as a modulation format on top of those reported in Section III-B. Additionally, the TC encapsulation can include multiple TC frames per CLTU. Finally, both ECSS and CCSDS allow either the use of BCH or LDPC coding. However, ECSS allows BCH for single error detection only, while CCSDS foresees BCH also for triple error detection.
- *TM coding and synchronization*: CCSDS considers the RS code having a rate of 239/255 (see Section III-C) as a general coding option, while ECSS allows the RS 239/255 only when the TM signal is 8PSK-TCM;
- *Tracking*: code ranging is not a CCSDS standard, while PN ranging is CCSDS only. For PN ranging, CCSDS foresees the blue book [40], complemented by the recommendation 2.5.5A in [25]. The related green book is instead [41]. Then, CCSDS allows the simultaneous transmission of PN ranging with GMSK, as reported in [25], recommendations 2.4.22A and 2.4.22B;
- Finally, also the following standards are part of CCSDS and not of ECSS: DDOR (recommendations 2.5.6B in [25]), VCM (blue books [51], [52], [77] and green books [54], [78]) and telemetry ranging (recommendation 2.4.24 in [25]).

It is worth pointing out that, although not yet standards, CCSDS currently has two experimental definitions for an extension of VCM up to 256APSK, as provided in the orange books [79], [80]. Additionally, CCSDS is planning to

have dedicated recommendations for K-Band uplink and WB-DDOR, with the approach described in Section V.

### C. SFCG & ITU

The space frequency coordination group (SFCG) was established to provide a less formal and more flexible environment, compared to the official organs of the ITU, for solving frequency management problems encountered by member space agencies. In naïve words, the SFCG deals exclusively with the spectrum management of frequency allocations for space systems, trying to cover and complement ITU regulations while finding a common position among space agencies concerning the assignment of specific frequencies and related technical issues.

The main output of SFCG are *technical resolutions and recommendations* [15]. These are usually short documents providing requirements or good practices for designing TT&C subsystems and units. The only difference between resolutions and recommendations is their applicability to projects done by member space agencies and other external bodies (e.g., commercial satellites). However, considering the challenges in spectrum management (e.g., see recent issues of 5G interference risks with EO satellites [81]), in the authors' opinion, the good TT&C engineer should always consider both resolutions and recommendations as mandatory requirements.

It is finally pointed out that SFCG recommendations are usually already covered by dedicated requirements in the ECSS standard in [11]. Hence (once again), ECSS is a good starting point. On the other hand, since ECSS is not always “up-to-speed” (especially for future Lunar and Martian missions), it is always recommended to the reader checking the SFCG website for the latest resolutions and recommendations.

## VII. CONCLUSIONS

This paper presented an in-depth tutorial on the TT&C for spacecraft, providing first an overview of the space system, and then describing the spacecraft TT&C subsystem, its physical layer, and its main units. These basics have been complemented with a description of the most recent techniques

and technologies in the field, and with an overview of the standardization organization.

This paper should help the engineering community get familiar with the world of the TT&C, often considered a specialized professional field for a few people.

## REFERENCES

- [1] P. Foterscue, G. Swinerd, and J. Stark, *Spacecraft systems engineering*. John Wiley & Sons, 4th ed., 2011.
- [2] NASA, "NASA Systems Engineering Handbook." Available at [www.nasa.gov/connect/ebooks/nasa-systems-engineering-handbook](http://www.nasa.gov/connect/ebooks/nasa-systems-engineering-handbook), 2020.
- [3] ITU, "Radio Regulations," June 2016. Available at [handle.itu.int/11.1002/pub/80da2b36-en](http://handle.itu.int/11.1002/pub/80da2b36-en).
- [4] Copernicus Earth Observation Programme, "Sentinels." Website: [www.esa.int/Applications/Observing\\_the\\_Earth](http://www.esa.int/Applications/Observing_the_Earth).
- [5] European Space Agency and Chinese Academy of Science, "Solar wind magnetosphere ionosphere link explorer (SMILE)." Website: [sci.esa.int/web/smile](http://sci.esa.int/web/smile).
- [6] European Space Agency, "Cosmos: The portal for users of esa's science directorate's missions." Website: [www.cosmos.esa.int](http://www.cosmos.esa.int).
- [7] ESA EO Portal, "Solar Orbiter Mission." Website: <https://directory.eoportal.org/web/eoportal/satellite-missions/s/solar-orbiter-mission>.
- [8] European Space Agency, "In-orbit servicing active debris removal." Website: [www.esa.int/Safety\\_Security/Clean\\_Space/in-orbit\\_servicing\\_active\\_debris\\_removal](http://www.esa.int/Safety_Security/Clean_Space/in-orbit_servicing_active_debris_removal).
- [9] G. F. Dubos, J. H. Saleh, and R. Braun, "Technology readiness level, schedule risk, and slippage in spacecraft design," *Journal of Spacecraft and rockets*, vol. 45, pp. 836–842, July 2008.
- [10] ECSS-E-HB-11A, Space Engineering - Technology Readiness level (TRL) guidelines, March 2017. Available at [www.ecss.nl](http://www.ecss.nl).
- [11] ECSS-E-ST-50-05C, Space Engineering - Radio frequency and modulation, October 2011. Available at [www.ecss.nl](http://www.ecss.nl).
- [12] J. P. Laboratory, *Deep Space Network Services Catalog*. 2015. Available at [deepspace.jpl.nasa.gov](http://deepspace.jpl.nasa.gov).
- [13] ESOC, *ESTRACK Facilities Manual*. 2017. Available on request at <http://estracknow.esa.int>.
- [14] M. Maniewicz, "Outcome of the world radiocommunication conference, 2015," in *Proc. Dynamic Spectral Allocation (DSA) Global Summit*, (Bogota, Columbia), Apr. 2015.
- [15] SFCG, "Resolutions and Recommendations," 2022. Available at [www.sfcgonline.org](http://www.sfcgonline.org).
- [16] F. Tonicello, B. Mauret, H. Jensen, L. Croci, N. Deplus, N. Neugnot, P. Rumler, and T. Kocma, "ECSS-E-ST&HB-20-20C – A power interface standard & handbook for products development," in *Proc. E3S Web of Conferences*, 2017.
- [17] A. Papoulis, *Probability, Random Variables and Stochastic Processes*. New York, NY: McGraw-Hill, 1991.
- [18] Copernicus Earth Observation Programme, "Sentinel-1 - The SAR Imaging Constellation for Land and Ocean Services." Website: <http://eoportal.org/web/eoportal/satellite-missions/c-missions/copernicus-sentinel-1>.
- [19] G. Minatti, S. Maci, P. De Vita, A. Freni, and M. Sabbadini, "A circularly-polarized isoflux antenna based on anisotropic metasurface," *IEEE Trans. Antennas and Prop.*, vol. 60, no. 11, pp. 4998–5009, 2012.
- [20] I. Shurmer, F. Marchese, and J. Morales, "Sentinels optical communications payload (OCP) operations: From test to in-flight experience," in *Space Operations Organization Conference (SpaceOps)*, (Marseille, France), May 2018.
- [21] G. D. Racca, R. Laureijs, L. Stagnaro, J.-C. Salvignol, J. L. Alvarez, G. S. Criado, L. G. Venancio, A. Short, P. Strada, T. Bönke, et al., "The Euclid mission design," in *Space Telescopes and Instrumentation 2016: Optical, Infrared, and Millimeter Wave*, vol. 9904, p. 99040O, International Society for Optics and Photonics, 2016.
- [22] M. K. Simon and S. Million, "Residual versus suppressed-carrier coherent communications," *NASA TDA Progress Report*, vol. 42, p. 127, 1996.
- [23] R. De Gaudenzi, A. Guillén i Fabregas, and A. Martinez, "Performance analysis of turbo-coded APSK modulations over nonlinear satellite channels," *IEEE Trans. Wireless Commun.*, vol. 5, pp. 2396–2407, Sept. 2006.
- [24] K. Murota and K. Hirade, "GMSK modulation for digital mobile radio telephony," *IEEE Trans. Commun.*, vol. 29, pp. 1044–1050, July 1981.
- [25] CCSDS 401.0-B-30, Radio frequency and modulation systems, Part 1, Feb. 2020. Available at <http://public.ccsds.org/>.
- [26] CCSDS 413.0-G-3, Bandwidth-Efficient Modulations - Summary of definition, implementation, and performance, Feb. 2018. Available at <http://public.ccsds.org/>.
- [27] M. Abramowitz and I. A. Stegun, eds., *Handbook of Mathematical Functions*. Dover, 1972.
- [28] ECSS-E-AS-50-24C, Adoption Notice of CCSDS 231.0-B-3, TC Synchronization and Channel Coding, March 2021. Available at [www.ecss.nl](http://www.ecss.nl).
- [29] R. C. Bose and D. K. Ray-Chaudhuri, "On a class of error correcting binary group codes," *Information and control*, vol. 3, no. 1, pp. 68–79, 1960.
- [30] R. G. Gallager, "Low density parity check codes," *IEEE Trans. Inform. Theory*, vol. 8, pp. 21–28, Jan. 1962.
- [31] CCSDS 231.0-B-4, TC synchronization and channel coding, July 2021. Available at <https://public.ccsds.org/>.
- [32] ECSS-E-AS-50-25C, Adoption Notice of CCSDS 232.0-B-3, TC Space Data Link Protocol, March 2021. Available at [www.ecss.nl](http://www.ecss.nl).
- [33] CCSDS 230.1-G-3, TC Synchronization and Channel Coding - Summary of Concept and Rationale, Oct. 2021. Available at <http://public.ccsds.org/>.
- [34] ECSS-E-ST-50C, Space Engineering - Communications, July 2008. Available at [www.ecss.nl](http://www.ecss.nl).
- [35] CCSDS 232.0-B-3, TC space data link protocol, Sept. 2015. Available at <https://public.ccsds.org/>.
- [36] ECSS-E-AS-50-21C, Adoption Notice of CCSDS 131.0-B-3, TM Synchronization and Channel Coding, March 2021. Available at [www.ecss.nl](http://www.ecss.nl).
- [37] CCSDS 131.0-B-4, TM synchronization and channel coding, Apr. 2022. Available at <http://public.ccsds.org/>.
- [38] ECSS-E-AS-50-22C, Adoption Notice of CCSDS 132.0-B-2, TM Space Data Link Protocol, March 2021. Available at [www.ecss.nl](http://www.ecss.nl).
- [39] ECSS-E-ST-50-02C, *Ranging and Doppler Tracking*, July 2008. Available at [www.ecss.nl](http://www.ecss.nl).
- [40] CCSDS 414.1-B-2, Pseudo-Noise PN Ranging Systems, Feb. 2012. Available at <http://public.ccsds.org/>.
- [41] CCSDS 414.0-G-2, Pseudo-Noise PN Ranging Systems, Feb. 2014. Available at <http://public.ccsds.org/>.
- [42] CCSDS 413.1-G-2, Simultaneous transmission of GMSK telemetry and PN Ranging, Nov. 2017. Available at <https://public.ccsds.org/>.
- [43] H. Friis, "A note on a simple transmission formula," *Proceedings of the IRE*, vol. 34, no. 5, pp. 254–256, 1946.
- [44] Centre national d'études spatiales, "PROPA: Dynamic link library PROPAGATION." Available at <https://logiciels.cnes.fr/en/content/propa>.
- [45] J. H. Yuen, "A practical statistical model for telecommunications performance uncertainty," tech. rep., 1975.
- [46] F. M. Gardner, *Phase-lock techniques*. Wiley-Interscience, 3rd ed., 2005.
- [47] J. Vilà-Valls, M. Navarro, P. Closas, and M. Bertinelli, "Synchronization challenges in deep space communications," *IEEE Aerospace and Electronic Systems Magazine*, vol. 34, no. 1, pp. 16–27, 2019.
- [48] Y. Luo, Y. Wang, Y. Ha, Z. Wang, S. Chen, and H. Pan, "Generalized hyperbolic cordic and its logarithmic and exponential computation with arbitrary fixed base," *IEEE Trans. VLSI*, vol. 27, no. 9, pp. 2156–2169, 2019.
- [49] European Space Agency, "International workshop on tracking, telemetry, and command for space," (Noordwijk, The Netherlands), Dec. 2022.
- [50] Tesat-Spacecom and Kongsberg Spacotec, *FleXLink: Multi-Gigabit Data Downlink End-to-End Chain. White Paper: Maximizing Throughput in Satellite to Ground Transmissions*. Backnang, Germany and Tromsø, Norway, June 2017.
- [51] CCSDS 431.1-B-1, Variable Coded Modulation Protocol, Feb. 2021. Available at <http://public.ccsds.org/>.
- [52] CCSDS 131.2-B-2, Flexible advanced coding and modulation scheme for high rate telemetry applications, Apr. 2022. Available at <http://public.ccsds.org/>.
- [53] A. Modenini, A. Ugolini, and G. Colavolpe, "A fast method for optimizing the amplifier output back-off by means of the total degradation," in *International Workshop on Tracking, Telemetry, and Command for Space*, (Darmstadt, Germany), Sept. 2019.
- [54] CCSDS 130.11-G-1, SCCC-Summary of definition and performance, Apr. 2019. Available at <https://public.ccsds.org/>.
- [55] R. Carbone, N. Salerno, F. Marcelli, E. Rondoni, R. Cassettari, J. G. Villarino, J. J. Rigau, and A. Modenini, "High rate flexible high-order SCCC communications system for science X-band," in *International Workshop on Tracking, Telemetry, and Command for Space*, (Noordwijk, The Netherlands), Dec. 2022.

- [56] M. Cossu, G. Montorsi, M. Bertinelli, M. Visintin, A. Bicchieri, and N. Jeannin, "Adaptive coding modulation for Earth observation satellites in leo orbit," in *Space Operations Organization Conference (SpaceOps)*, (Daejeon, South Korea), May 2016.
- [57] M. Visintin, G. Montorsi, M. Cossu, and N. Jeannin, "Algorithms for the implementation of adaptive coding modulation on Earth observation satellites," in *International Workshop on Tracking, Telemetry, and Command for Space*, (Noordwijk, The Netherlands), Nov. 2016.
- [58] M. Davidson, N. Gebert, and L. Giulicchi, "ROSE-L – the L-band SAR mission for Copernicus," in *European Conference on Synthetic Aperture Radar (EUSAR)*, (held virtually), Mar. 2021.
- [59] CCSDS 720.1-G-3, *CCSDS File Delivery protocol (CFDP) - Part 1: introduction and overview*, Apr. 2007. Available at <https://public.ccsds.org/>.
- [60] R. Roscigno, S. Fenu, E. Tirro, S. D'Amico, F. Spataro, S. Osborne, and A. Modenini, "Payload data handling & transmission system on ROSE-L mission: main features and CFDP protocol application for data downlink," in *Workshop on RF and Microwave Systems, Instruments & Sub-systems and Ka-band Workshop*, (Noordwijk, The Netherlands), Jan. 2022.
- [61] S. Pavale, E. Unnikrishnan, and P. Lakshminarasimhan, "Design, implementation and performance evaluation of CCSDS CFDP protocol," in *Proc. IEEE Intern. Conf. on Computational Intelligence and Computing Research*, (Coimbatore, India), Jan. 2010.
- [62] B. Ripani, A. Modenini, and G. Montorsi, "On the use of PN ranging with high-rate spectrally-efficient modulations in satellite payload telemetry links," *IEEE Trans. on Aerospace and Electronic Systems*, pp. 1–1, May 2022.
- [63] L. Lomidze, D. J. Knudsen, J. Burchill, A. Kouznetsov, and S. C. Buchert, "Calibration and validation of Swarm plasma densities and electron temperatures using ground-based radars and satellite radio occultation measurements," *Radio Science*, vol. 53, pp. 15–36, Jan. 2018.
- [64] J. S. Border and J. A. Koukos, "Technical characteristics and accuracy capabilities of delta differential one-way ranging (DeltaDOR) as a spacecraft navigation tool," *JPL Technical Report*, 1993. Available at <https://trs.jpl.nasa.gov/>.
- [65] C. P. Volk, "Sample transponder implementations for PN DDOR," *JPL Technical Report*, 2020. Available at <https://trs.jpl.nasa.gov/>.
- [66] K. Andrews, J. Hamkins, S. Shambayati, and V. Vilnrotter, "Telemetry-based ranging," in *Proc. IEEE Aerospace Conf.*, Mar. 2010.
- [67] V. Vilnrotter, J. Hamkins, and S. Ashrafi, "Performance analysis of digital tracking loops for telemetry-based ranging applications," in *Proc. IEEE Aerospace Conf.*, Mar. 2014.
- [68] J. Hennawy, N. Adams, E. Sanchez, D. Srinivasan, J. Hamkins, V. Vilnrotter, H. Xie, and P. Kinman, "Telemetry ranging using software-defined radios," in *Proc. IEEE Aerospace Conf.*, Mar. 2015.
- [69] B. Hespeler, H. Hofmann, A. Camuso, J. Lange, and A. Modenini, "Integrated X-Band payload data transmitter & TTC transponder (IXPT)," in *International Workshop on Tracking, Telemetry, and Command for Space*, (Noordwijk, The Netherlands), Nov. 2022.
- [70] N. Salerno, L. Simone, D. Gelfusa, M. Belardinelli, M. Salvati, and R. Viola, "TT&C transponder with integrated payload data transmitter for Earth Observation missions," in *International Workshop on Tracking, Telemetry, and Command for Space*, (Noordwijk, The Netherlands), Nov. 2022.
- [71] A. Aroumont, P. Maguire, B. Hespeler, E. Couty, and S. Carrasco Martos, "Very high data rate receiver for K-band uplink for future Moon exploration missions," in *International Workshop on Tracking, Telemetry, and Command for Space*, (Noordwijk, The Netherlands), Nov. 2022.
- [72] F. Pelorossi, F. Concaro, I. Montesinos, M. Pasian, and C. Chambon, "Implementation of the K-band uplink channel for Moon missions in the existing ESA deep space antennas," in *International Workshop on Tracking, Telemetry, and Command for Space*, (Noordwijk, The Netherlands), Nov. 2022.
- [73] S. Marti and E. Vassallo, "Future multiple uplink per aperture access schemes," in *Space Operations Organization Conference (SpaceOps)*, (Stockholm, Sweden), June 2012.
- [74] D. Gelfusa, C. F., N. Salerno, and L. Simone, "Integrated deep space & radio-science TT&C transponder (IDST)," in *International Workshop on Tracking, Telemetry, and Command for Space*, (Darmstadt, Germany), Sept. 2019.
- [75] C. Campa, D. Gianfelici, and R. Abello, "Multiple spacecraft per aperture with code division multiple access modulation," in *International Workshop on Tracking, Telemetry, and Command for Space*, (Noordwijk, The Netherlands), Dec. 2022.
- [76] CCSDS 130.1-G-3, *TM Synchronization and Channel Coding - Summary of Concept and Rationale*, June 2020. Available at <http://public.ccsds.org/>.
- [77] CCSDS 131.3-B-2, *CCSDS Space Link Protocols over ETSI DVB-S2 Standard*, Apr. 2022. Available at <http://public.ccsds.org/>.
- [78] CCSDS 130.12-G-1, *CCSDS Protocols over DVB-S2 - Summary of Definition, Implementation, and Performance*, Nov. 2016. Available at <https://public.ccsds.org/>.
- [79] CCSDS 131.21-O-1, *Serially Concatenated Convolutional Codes - Extension (SCCC-X)*, May 2021. Available at <https://public.ccsds.org/>.
- [80] CCSDS 131.31-O-1, *CCSDS Space Link Protocols over ETSI DVB-S2X Standard*, Sept. 2021. Available at <https://public.ccsds.org/>.
- [81] A. Witze, "Global 5G wireless deal threatens weather forecasts," *Nature*, vol. 575, pp. 577–578, Nov. 2019.



**Andrea Modenini** was born in Parma, Italy, in 1986. He received the MSc in Telecommunications Engineering (cum laude) on December 13, 2010, and the Ph.D. in January 2014 from the University of Parma.

Since March 2015, he is at the European Space Agency (ESA), currently working as TT&C Communications Systems Engineer, supporting ESA Earth Observation and Scientific satellite missions, research and development of TT&C units, techniques, including the command and control (C2) for unmanned aerial vehicles (UAVs). He is also contributing to the education in the field of TT&C as tutor of ESA trainees. Finally, he is involved in several standardization activities for satellite TT&C in the framework of ECSS, SFCG, and CCSDS. For the latter, he is Chair of the Coding & Synchronization working group.

In 2014 he was postdoctoral researcher at the Dipartimento di Ingegneria dell'Informazione (DII) in Professor Giulio Colavolpe research group. In spring 2012 he was a visiting PhD student in the group of Prof. Fredrik Rusek of the Elektro- och informationsteknik of the University of Lund, Sweden.

In June 2014 he won the award issued by GTTI for the best PhD thesis, in the field of telecommunications, discussed in Italy.

He served also as a Technical Program Committee (TPC) member for ASMS/SPSC 2012 and 2014, and as the main organizer and TPC chair of the ESA international workshop on TT&C in 2022.



**Barbara Ripani** received her Bachelor's Degree from Università Politecnica Delle Marche in Biomedical Engineering in 2018 and her Master's Degree from Politecnico di Torino in Communications and Computer Networks Engineering in 2021. She carried out her Master's Degree thesis at the European Space Research Technology Center (ESTEC) on coupling Pseudo-Noise ranging with high-order modulated telemetry signals, followed by a post-graduate traineeship. During this period, she gained experience designing TT&C and PDT subsystems

for space missions in early phases, supported satellite assembly, integration, and testing activities, and got involved in standardization activities. She is working toward the Ph.D., started in September 2021 at Politecnico di Torino, under the supervision of Prof. Guido Montorsi and Ph.D. Andrea Modenini. Currently, she is working as a contractor in ESTEC. Her research topic focuses on synchronization challenges in Deep Space communication links. In January 2022, she became a student member of IEEE, AESS, and ComSoc societies.